

DTIC FILE COPY

AD-A203 289



DTIC
 JAN 18 1989
 S H D

A POSITION, SCALE, AND ROTATION INVARIANT
 HOLOGRAPHIC ASSOCIATIVE MEMORY

THESIS

Kenneth Henry Fielding
 Captain, USAF

AFIT/GEO/ENG/88D-2

DEPARTMENT OF THE AIR FORCE
 AIR UNIVERSITY

AIR FORCE INSTITUTE OF TECHNOLOGY

Wright-Patterson Air Force Base, Ohio

DISTRIBUTION STATEMENT A

Approved for public release;
 Distribution Unlimited

89

1 17 151

AFIT/GEO/ENG/88D-2

A POSITION, SCALE, AND ROTATION INVARIANT
HOLOGRAPHIC ASSOCIATIVE MEMORY

THESIS

Kenneth Henry Fielding
Captain, USAF

AFIT/GEO/ENG/88D-2

DTIC
EL E
S JAN 18 1989 D
9 H

Approved for public release; distribution unlimited

AFIT/GEO/ENG/88D-2

**A POSITION, SCALE, AND ROTATION INVARIANT
HOLOGRAPHIC ASSOCIATIVE MEMORY**

THESIS

**Presented to the Faculty of the School of Engineering
of the Air Force Institute of Technology
Air University
In Partial Fulfillment of the
Requirements for the Degree of
Master of Science in Electrical Engineering**

**Kenneth Henry Fielding, B.S.,B.S.E.E.
Captain, USAF**

December 1988

Approved for public release; distribution unlimited

Preface

The purpose of this study is to investigate and characterize the Hughes Research Corporation's holographic associative memory. A position, scale, and rotation invariant version of this memory is described. This research is sponsored, in part, by RADC/COTC and contributes to the Air Force's on-going investigation of autonomous pattern recognition systems.

I have received an enormous amount of help and encouragement while working on this thesis. I sincerely thank my thesis advisor, Capt (Dr.) Steven K. Rogers, for his patience and understanding help with every aspect of this thesis research. I also thank the members of my thesis committee, Dr. Matthew Kabrisky and Lt Col (Dr.) James P. Mills, for their guidance and helpful suggestions throughout this effort. My deep gratitude goes to Capt Jeff Wilson for his many insightful comments along the way.

Most importantly, I thank my wife, [REDACTED]. Her encouragement, help, and understanding made this thesis effort and the entire Master's Program a success for myself and my family.

Kenneth Henry Fielding



Accession For	
NTIS GRA&I	<input checked="" type="checkbox"/>
DTIC TAB	<input type="checkbox"/>
Unannounced	<input type="checkbox"/>
Justification	
By _____	
Distribution/	
Availability Codes	
and/or	Special
A-1	

Table of Contents

	Page
Preface	ii
Table of Contents	iii
List of Figures	vi
List of Tables	viii
Abstract	ix
I. Introduction	1
1.1 Summary of Current Knowledge	1
1.2 Problem Definition	4
1.3 Approach	4
II. The Holographic Associative Memory	6
2.1 Introduction	6
2.2 The Single Iteration Memory	7
2.2.1 Number of Stored Objects	12
2.3 Summary	12
III. The Position, Scale, and Rotation Invariant Feature Space	14
3.1 Introduction	14
3.2 The $ F(f_{Inr}, f_{\theta}) $ Feature Space	15
3.2.1 Introduction	15
3.2.2 Theory	15

	Page
IV. The Phase Conjugate Mirror	19
4.1 Introduction	19
4.2 Background	19
4.3 Coupling Strength	21
4.4 The Experiment	24
4.4.1 Experimental Results	26
4.5 Summary	30
V. The Hologram	31
5.1 Introduction	31
5.2 The Holographic Plates	31
5.3 The Kodak HRP 1-A Plates	31
5.4 Summary	37
VI. The Experiment	38
6.1 Introduction	38
6.2 The Design	38
6.2.1 Exposure of the Holographic Plates	40
6.3 Experimental Results	40
6.3.1 Shift Invariance Experiment	42
6.3.2 Artificial Diffusers	44
6.3.3 Demonstration of Distortion Invariance	45
6.4 Summary	46
VII. Conclusions and Recommendations	48
7.1 Conclusions	48
7.1.1 Future Applications	48
7.2 Recommendations	49

	Page
Appendix A. The Computer Generated Hologram	50
A.1 Introduction	50
A.2 Background and Generation	50
A.3 The computer program	54
Appendix B. Samples of the PSRI Feature Space	57
B.1 Introduction	57
Bibliography	64
Vita	66

List of Figures

Figure	Page
1. Single Iteration Holographic Associative Memory.	3
2. Hologram Recording Method.	7
3. The Holographic Associative Memory.	9
4. $ F(f_{inr}, f_{\theta}) $ Generation Method.	18
5. Phase Conjugate Beam Path.	20
6. Coupling Constant.	23
7. PCM Reflectivity Experiment.	25
8. Phase Conjugate Reflectivity.	26
9. Photograph of the PCM.	27
10. Phase Conjugate Oscillation.	28
11. Phase Conjugate Return of the Resolution Chart.	29
12. Recording of Plane Waves.	32
13. Experimental t-E Curve for Kodak 1-A Plates.	35
14. Diffraction Efficiency of Bleached Holograms.	36
15. Hologram Recording Method for the HAM.	39
16. The Holographic Associative Memory.	41
17. The Triangle and its Associative Output.	43
18. An F-15 and Tape and its Output.	45
19. An F-15 With Tape Removed and the Associated Output.	46
20. Laser Printer Plot of the CGH.	52
21. Dekacon Setup.	53
22. The Large Square.	57
23. The Small Square.	58
24. The Small Square Rotated 45 Degrees.	58

Figure	Page
25. The Triangle Normal and Rotated 30 Degrees.	59
26. The Small Tank.	59
27. The Large Tank.	60
28. The Truck and Tank at 90 Degrees.	60
29. The Small F-15.	61
30. Two Trucks and Two Tanks.	61
31. Truck, Tank, and F-15.	62
32. The Large Edged Square.	62
33. The Small Edged Square.	63

List of Tables

Table	Page
1. Internal Crystal Angles.	24

Abstract

This thesis investigates an all-optical position, scale, and rotation invariant (PSRI) holographic associative memory employing phase conjugation. The PSRI feature space is the ln-polar representation of the magnitude of the Fourier transform, $|F(f_{lnr}, f_{\theta})|$, of the objects. This representation is generated using a coordinate transform computer generated hologram. Diffuse Fourier transform holograms of the PSRI feature space and the use of angularly multiplexed references allow access to the correlation domain where the nonlinear properties of the phase conjugate mirror, self pumped $BaTiO_3$, reduces cross-correlation noise and provides object discrimination. The self-pumped phase conjugate mirror is characterized and a procedure for consistent production of high diffraction efficiency holograms is developed. The holographic associative memory is constructed and its operational parameters are defined.

One object is stored in the memory because of limitations on the size of the Fourier transforming optic and the properties of the ground glass diffuser. Fast optics and a custom designed phase diffuser are recommended to alleviate this system characteristic.

*Submitted to the Faculty of the Graduate School of the Air Force Institute of Technology
in partial fulfillment of the requirements for the degree of
Doctor of Philosophy
August 1988*

A POSITION, SCALE, AND ROTATION INVARIANT HOLOGRAPHIC ASSOCIATIVE MEMORY

I. Introduction

Automatic, real-time pattern recognition is a major concern of the Air Force in the areas of pilot aids, smart weapons, and general purpose robotics[16:1]. A pattern recognition device that works in real-time and can operate independent of object position, scale, and in-plane rotation, is needed to accurately find targets in their natural surroundings. For the most part, pattern recognition is done on large computer systems using algorithms that require an enormous amount of calculation time. Optical pattern recognition can be performed in parallel and at high speeds measured in nanoseconds.

The advantage of high speed performance makes the use of optical systems appealing for real-time pattern recognition. This research is part of the Air Force's ongoing investigation into the basic characteristics of a specific type of optical pattern recognition device, the holographic associative memory (HAM).

1.1 Summary of Current Knowledge

An associative memory may be defined as a fault-tolerant content-addressable memory which can recall complete noise-free objects when addressed by partial or distorted input objects[18:1900]. Pattern recognition done by coherent optical processors, in particular those based on holographic principles, are well suited to associative processing. Optical processors allow for parallel processing, global interconnections, and high speed calculations. The hologram is the memory device in the

HAM. This memory device can be homoassociative or heteroassociative, recalling a like or different object when addressed with a specific input.

Elementary versions of the holographic associative memory have been limited in storage capacity and achievable signal-to-noise ratio (SNR) because of correlation cross-talk between the stored objects. Ghost image experiments of Collier and Pennington [4] as well as Marom and Goodman [15] demonstrated the association of one object pair.

Recently both linear and ring resonator configurations of a holographic associative memory have been reported by Owechko, Dunning, Marom, and Soffer [18], D.Z. Anderson [1], White, Aldridge, and Lindsay [22], and Yariv and Kwong [25]. Owechko et al. are the leading investigators of holographic associative memories employing nonlinearities in the correlation domain. These nonlinearities provide gain and feedback that improve system performance. Owechko et al. describe three memory systems in detail: (1) the holographic analog to the outer-product model of a neural network, (2) a multiple iteration nonlinear holographic associative memory, and (3) a single iteration nonlinear holographic associative memory. A great deal of research has been done using the single iteration memory. Dunning et al. have shown the memory can recall objects when presented with as little as 20 percent of one of the stored objects [8:348]. These objects were geometric figures, words, and a grey scale image. This thesis focuses on the single iteration holographic associative memory which is shown in Figure 1.

A brief operational definition of the memory follows. The hologram is "charged" with the desired stored objects each exposed with its unique angle multiplexed reference. The hologram is then placed into the system shown in Figure 1. When a partial or distorted version of one of the stored objects is presented at the input, the cross-correlation of that input with all stored objects leaves the hologram and its Fourier transform is directed toward the phase conjugate mirror (PCM). The PCM senses which beam has the strongest intensity and conjugates it while suppressing all

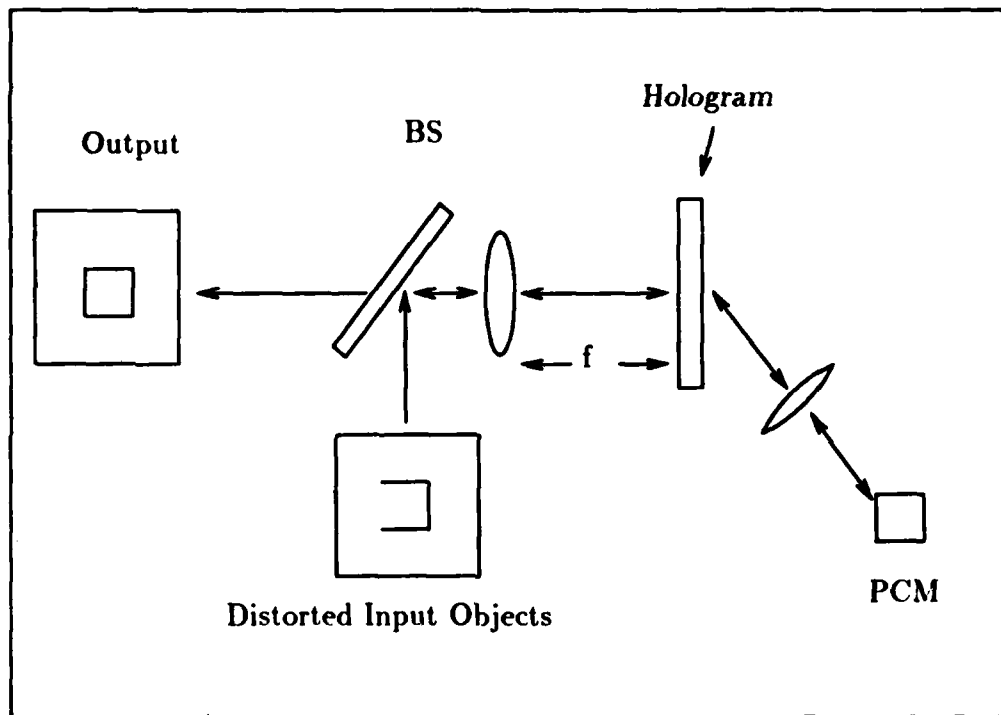


Figure 1. Single Iteration Holographic Associative Memory.

others. The hologram is reilluminated with the Fourier transform of this conjugated and thresholded reference corresponding to only one stored object, which is then seen at the output. A detailed investigation of the memory is presented in the next chapter.

The major difficulty of the present memory is that it is very sensitive to scales and rotations of the stored objects at the input. This is due to the memory being a classical Vander Lugt type optical correlator. Correlators, in general, are inherently sensitive to scale and in-plane rotational changes of the input objects. Input object scale changes of 2 percent and in-plane rotations of up to 3.5 degrees can cause SNR reductions of 27 dB, severely degrading correlator performance [2:1795]. A new feature space invariant to scales and rotations must be found to eliminate this difficult problem. The invariant feature space used is the ln-polar coordinate transform of

the magnitude of the Fourier transform, $|F(f_{lnr}, f_{\theta})|$.

1.2 Problem Definition

This thesis problem is to investigate the Hughes Research Corporation's holographic associative memory and implement a position, scale, and rotation invariant version using a self-pumped phase conjugator rather than a degenerate four wave mixing (DFWM) PCM.

The barium titanate, $BaTiO_3$, crystal must first be characterized as a self-pumped phase conjugate mirror and a method for producing high diffraction efficiency holograms must be developed to implement and characterize the Hughes HAM. The remainder of the thesis is devoted to developing a position, scale, and in-plane rotation invariant feature space to implement the PSRI holographic associative memory. The PSRI feature space is the ln-polar representation of the magnitude of the Fourier transform, $|F(f_{lnr}, f_{\theta})|$, of the objects. In the $|F(f_{lnr}, f_{\theta})|$ feature space, input scale changes are mapped into shifts on the f_{lnr} axis while rotations of the input are mapped into shifts on the f_{θ} axis. Position invariance is gained by using the magnitude of the Fourier transform. This system must be able to recall complete noise free templates from scaled and rotated input scenes.

1.3 Approach

This research is accomplished in three main parts.

Part one: thoroughly investigate the principle components of the holographic associative memory. Techniques for recording and developing holograms will be investigated giving careful consideration to exposure time, beam energies, and reference beam angles [3:269]. Self-pumped phase conjugation experiments in $BaTiO_3$ are performed to characterize its phase conjugate reflectivity [9:486]. The PSRI feature space is generated by inputting the desired objects magnitude of the Fourier

transform into a coordinate transform computer generated hologram. The $|F(f_{lnr}, f_{\theta})|$ representation is photographed and transferred to glass slides.

Part two: reaccomplish the single-iteration experiments of Owechko et al., determining the physical limitations of this system. The maximum amount of allowable scale and rotation changes as well as the amount of allowable input object distortion for several stored objects will be investigated.

Part three: implement the position, scale, and in-plane rotation invariant version of the memory. Known $|F(f_{lnr}, f_{\theta})|$ versions of the test objects will be stored on the hologram using angle multiplexing and diffuser techniques. The system performance is based on its ability to recall a noise free test object when addressed with the following: (1) a distorted version of a stored object, (2) a normal version of a scaled, rotated or scaled and rotated stored object, and (3) a distorted scaled, rotated, or scaled and rotated stored object. Up to three objects will be stored on a hologram, assessing system performance with single and multiple stored objects.

The major topics to be covered in this thesis by chapter are:

1. The holographic associative memory.
2. The PSRI feature space.
3. The phase conjugate mirror.
4. The hologram.
5. The experiment and result.
6. Conclusions and recommendations.

II. The Holographic Associative Memory

2.1 Introduction

Associative memories are fault-tolerant content-addressable memories that can recall complete objects from partial or distorted inputs. An associative memory based on holography can be homoassociative or hetroassociative, recalling like or different objects than the input. Optical memories have a distinct advantage in speed and process in a highly parallel manner. Because of these features, the optical associative memory is becoming very popular.

Previous versions of the holographic memory have been limited in storage capacity and SNR primarily because of the cross-correlation noise between stored objects [18:1900]. Owechko et al. [18] have investigated both linear and ring resonator versions of the holographic memory using both gain and feedback to increase performance. The SNR is improved by using angle multiplexed holography to store the desired objects. The cross-correlation noise associated with the multiplexed objects is reduced by employing nonlinearities in the correlation domain. This nonlinearity in the correlation domain is a phase conjugate mirror (PCM) which conjugates and thresholds the multiple reference beams produced at the hologram. The thresholded beams then reilluminate the hologram and the output is seen.

The use of Fourier transform holograms makes the system self-referencing and partially shift invariant [18:1901]. The amount of shift invariance is related to the number of stored objects and their spatial extent. Diffuser encoding of the objects further increases the SNR by sharpening the autocorrelation peaks compared to the cross-correlations [3:390].

Owechko et al. [18] have had good success with a single iteration version of the holographic memory. The memory used in this thesis, the PSRI variant, is based on this configuration.

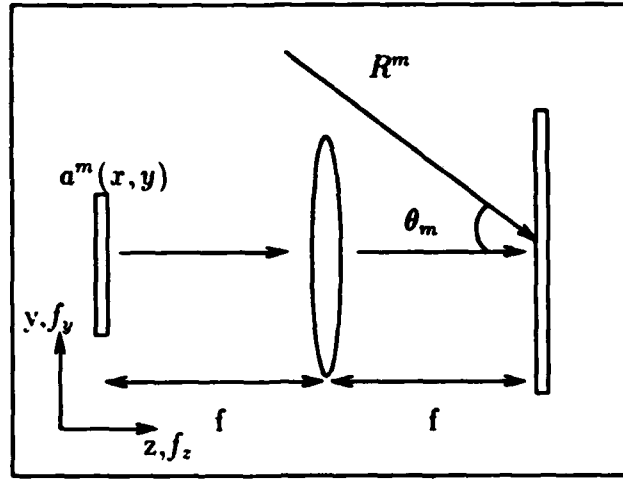


Figure 2. Hologram Recording Method.

2.2 The Single Iteration Memory

The most straight forward way to describe the memory is to give a step by step example of its operation beginning with the recording process. The recording method of the angle multiplexed hologram is shown in Figure 2.

In recording the hologram, a^m represents the m^{th} input object in the space domain (x, y, z) and $R^m(f_x, f_y) \exp^{j(\omega t - 2\pi(\alpha_m f_y + \gamma_m f_z))}$ its unique Gaussian plane wave reference in the Fourier domain (f_x, f_y, f_z) , at spatial frequencies $\alpha_m = \sin \theta_m / \lambda$ and $\gamma_m = \cos \theta_m / \lambda$. The optical frequency is ω . The total field at the hologram is during recording given by:

$$U_T^m(f_x, f_y) = R^m(f_x, f_y) \exp^{j(\omega t - 2\pi(\alpha_m f_y + \gamma_m f_z))} + A^m(f_x, f_y) \quad (1)$$

$A^m(f_x, f_y)$ is the Fourier Transform of a^m which is illuminated by a plane wave. The intensity on the holographic film is given by:

$$I(f_x, f_y) = \sum_m |U_T^m(f_x, f_y)|^2 \quad (2)$$

Substituting Equation 1 into Equation 2 yields:

$$I(f_x, f_y) = \sum_m |R^m(f_x, f_y) \exp^{j(\omega t - 2\pi(\alpha_m f_y + \gamma_m f_z))} + A^m(f_x, f_y)|^2 \quad (3)$$

Expanding and dropping the (f_x, f_y) notation and the temporal dependence:

$$I = \sum_m \left[|R^m|^2 + |A^m|^2 + A^m R^m \exp^{+j2\pi(\alpha_m f_y + \gamma_m f_z)} + \overline{A^m} R^m \exp^{-j2\pi(\alpha_m f_y + \gamma_m f_z)} \right] \quad (4)$$

Where $\overline{A^m}$ is the spatial complex conjugate. After the hologram is developed, Equation 4 becomes the transmittance given by:

$$\tau_f = \sum_m \beta'^m \left[|R^m|^2 + |A^m|^2 + A^m R^m \exp^{+j2\pi(\alpha_m f_y + \gamma_m f_z)} + \overline{A^m} R^m \exp^{-j2\pi(\alpha_m f_y + \gamma_m f_z)} \right] \quad (5)$$

Where:

$$\beta'^m = \beta^m \tau^m \begin{cases} \beta^m & \text{slope of the film t-E curve} \\ \tau^m & \text{exposure time} \end{cases} \quad (6)$$

Rewriting Equation 5 with $\beta'^m |R^m|^2$ being a uniform bias term τ_b^m :

$$\tau_f = \sum_m \left[\tau_b^m + \beta'^m |A^m|^2 + \beta'^m A^m R^m \exp^{+j2\pi(\alpha_m f_y + \gamma_m f_z)} + \beta'^m \overline{A^m} R^m \exp^{-j2\pi(\alpha_m f_y + \gamma_m f_z)} \right] \quad (7)$$

Equation 7 gives the total transmittance function for the storage of m objects on the holographic plate. This plate is put into the system shown in Figure 3.

The system is now presented with a partial or distorted version of one of the stored objects $\hat{a}^{m_0}(x, y)$ whose Fourier transform is $\hat{A}^{m_0}(f_x, f_y) \exp^{j(\omega t - 2\pi f_z/\lambda)}$. The term $\exp^{-j2\pi f_z/\lambda}$ in the exponent is dropped to ease the reading of the following equations. At the hologram there is the product of this transform and the transmittance

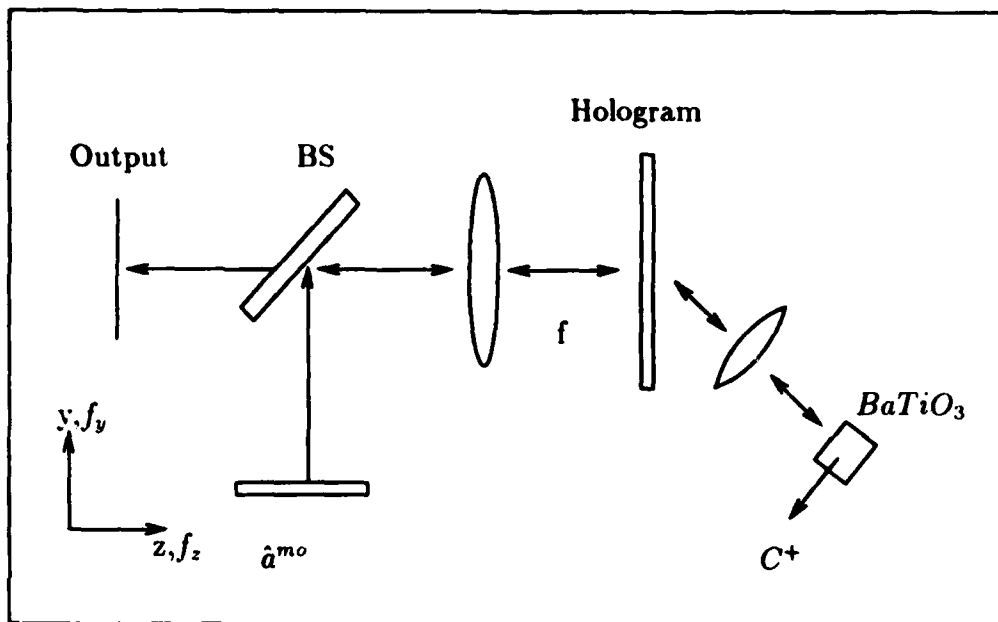


Figure 3. The Holographic Associative Memory.

τ_f to yield:

$$\hat{A}^{mo} \exp^{j\omega t} \sum_m \left[\tau_b^m + \beta'^m |A^m|^2 + \beta'^m A^m R^m \exp^{+j2\pi(\alpha_m f_y + \gamma_m f_z)} + \beta'^m R^m \overline{A^m} R^m \exp^{-j2\pi(\alpha_m f_y + \gamma_m f_z)} \right] \quad (8)$$

By the linearity of addition and summations Equation 8 can be rewritten in four terms as:

$$\begin{aligned} \hat{A}^{mo} \exp^{j\omega t} \tau_f &= \hat{A}^{mo} \exp^{j\omega t} \sum_m \tau_b^m \\ &+ \hat{A}^{mo} \exp^{j\omega t} \sum_m \beta'^m |A^m|^2 \\ &+ \hat{A}^{mo} \exp^{j\omega t} \sum_m \beta'^m A^m R^m \exp^{+j2\pi(\alpha_m f_y + \gamma_m f_z)} \\ &+ \hat{A}^{mo} \exp^{j\omega t} \sum_m \beta'^m \overline{A^m} R^m \exp^{-j2\pi(\alpha_m f_y + \gamma_m f_z)} \end{aligned} \quad (9)$$

The only terms of concern in Equation 9 are the ones that will propagate in the first diffracted order toward the phase conjugate mirror. The first two terms are

zero order terms traveling down the optical axis. The third term deflects "upward" at angle θ_m . The fourth term is the only one remaining. This term can be expanded to yield:

$$\hat{A}^{m_0} \exp^{j\omega t} \tau_f = \underbrace{\beta'^{m_0} \hat{A}^{m_0} \overline{A^{m_0}} R^{m_0} \exp^{j(\omega t - 2\pi(\alpha_{m_0} f_y + \gamma_{m_0} f_z))}}_{\text{Scaled "Auto-Reference"}} + \underbrace{\sum_{m \neq m_0} \beta'^m \hat{A}^{m_0} \overline{A^m} R^m \exp^{j(\omega t - 2\pi(\alpha_m f_y + \gamma_m f_z))}}_{\text{Cross-Reference Noise}} \quad (10)$$

If \hat{A}^{m_0} is close to A^m , the first term of Equation 10 is a recreation of the original reference used to expose the hologram, hence the name auto-reference. Equation 10 is Fourier transformed onto the phase conjugate mirror which performs a nonlinear threshold (NL) and phase conjugates the strongest components which hopefully come from the first term. The phase conjugate operation is performed on the temporal component of the exponential and is denoted by $*$. The general form of the phase conjugate return is:

$$NL \left[F \left(\sum_m \beta'^m \hat{A}^{m_0} \overline{A^m} R^m \exp^{j(\omega t - 2\pi(\alpha_m f_y + \gamma_m f_z))} \right) \right]^* \quad (11)$$

The phase conjugate return travels back along the same path as the beam incident on the crystal. The hologram is re-illuminated with the Fourier transform of Equation 11. The product of this term with the transmittance function τ_f of the hologram yields four terms which are given in the next four equations:

$$F \left[NL \left(F \left[\sum_m \beta'^m \hat{A}^{m_0} \overline{A^m} R^m \exp^{j(\omega t - 2\pi(\alpha_m f_y + \gamma_m f_z))} \right] \right) \right]^* \sum_n \tau_b^n \quad (12)$$

$$F \left[NL \left(F \left[\sum_m \beta'^m \hat{A}^{m_0} \overline{A^m} R^m \exp^{j(\omega t - 2\pi(\alpha_m f_y + \gamma_m f_z))} \right] \right) \right]^* \sum_n \beta'^n |A^n|^2 \quad (13)$$

$$F \left[NL \left(F \left[\sum_m \beta'^m \hat{A}^{m_0} \overline{A^m} R^m \exp^{j(\omega t - 2\pi(\alpha_m f_y + \gamma_m f_z))} \right] \right) \right]^* \sum_n \beta'^n A^n R^n \exp^{+j2\pi(\alpha_n f_y + \gamma_n f_z)} \quad (14)$$

$$F \left[NL \left(F \left[\sum_m \beta'^m \hat{A}^{m0} \overline{A^m} R^m \exp^{j(\omega t - 2\pi(\alpha_m f_y + \gamma_m f_z))} \right] \right)^* \right. \\ \left. \sum_n \beta'^n \overline{A^n} R^n \exp^{-j2\pi(\alpha_n f_y + \gamma_n f_z)} \right] \quad (15)$$

The only meaningful term is from Equation 14 since it contains a wavefront that travels in the $-z$ direction, opposite the original input wavefront. All other terms leave the hologram at different angles. Equation 14 undergoes another Fourier transform on its way to the output plane. Performing this Fourier transform on Equation 14 cancels the outside Fourier transform and results in:

$$NL \left(F \left[\sum_m \beta'^m \hat{A}^{m0} \overline{A^m} \exp^{j\omega t} \left(R^m \exp^{-j2\pi(\alpha_m f_y + \gamma_m f_z)} \right) \right] \right)^* \\ F \left[\sum_n \beta'^n A^n \left(R^n \exp^{+j2\pi(\alpha_n f_y + \gamma_n f_z)} \right) \right] \quad (16)$$

The only term from Equation 16 that travels down the optic axis is when the indices of the summation are the same, $m = n$, and the equation becomes:

$$NL \left(F \left[\beta'^m \hat{A}^{m0} \overline{A^m} \exp^{j\omega t} \left(R^m \exp^{-j2\pi(\alpha_m f_y + \gamma_m f_z)} \right) \right] \right)^* \\ F \left[\beta'^m A^m \left(R^m \exp^{+j2\pi(\alpha_m f_y + \gamma_m f_z)} \right) \right] \quad (17)$$

It is convenient to let $S^m = R^m \exp^{-j2\pi(\alpha_m f_y + \gamma_m f_z)}$, whose Fourier transform is s^m , and reinsert the term $\exp^{-j2\pi f_z/\lambda}$. Equation 17 then becomes:

$$NL \left(F \left[\beta'^m \hat{A}^{m0} \exp^{j(\omega t - 2\pi f_z/\lambda)} \overline{A^m} S^m \right] \right)^* F \left[\beta'^m A^m \overline{S^m} \right] \quad (18)$$

Assuming the crystal thresholded and reflected only the reference associated with the autocorrelation, performing the Fourier transforms in Equation 18 leads to the output of the memory, \hat{a}^{m0} :

$$\hat{a}^{m0} = \beta'^{m0} \left[\beta'^{m0} (\hat{a}^{m0} \star a^{m0}) \star s^{m0} \right] \star s^{m0} \star a^{m0} \quad (19)$$

If $\hat{a}^{m0} \approx a^{m0}$ then the correlation has a high narrow peak and the result is an "idealized" version of the original stored object, a^{m0} .

2.2.1 Number of Stored Objects The relationship of multiple stored objects and system performance is concisely described by Owechko et al. [18:1906-1907]. The following discussion is based on this reference. Owechko et al. reported having to replace input objects within $10\text{-}20\mu\text{m}$ of its original position, before using Fourier holograms, to satisfy the reconstruction requirements of a Fresnel hologram [18:1909]. This is the fundamental reason for going to the Fourier transform hologram and the previous statment that the system is self-referencing and partially shift invariant. The amount of permissible input shift without ambiguity in the output is limited by the angular separation of the multiple reference beams and the spatial widths of the stored objects. If all objects are centered when stored and the distorted input object is centered, the output of the memory will be centered. As the distorted input object is moved off center, a phase factor from the Fourier shift theorem is introduced, deflecting the reconstructed reference at a proportional angle. In turn, the output of the memory is shifted by an equal amount as the distorted input. When the input shift is large enough, the phase conjugated reference derived from the autocorrelation term reilluminates the hologram sending either a combination of stored objects, or and entirely different stored object toward the output of the memory. The amount of shift is directly tied to the spatial width of each stored object and the reference beam angles. Only one stored object can be moved over the entire input scene.

Owechko et al. have stored two objects on a thin hologram and successfully recalled each with a distorted version of the templates. Dunning has informally reported storing as many as 5 objects using LiNbO_3 as the memory element [7].

2.3 Summary

This chapter described the operational theory of the holographic associative memory. Equation 19 has shown how an idealized version of a stored object can be recalled when the system is presented with a partial or distored version of the

stored object. Dunning et al. recovered the proper stored object when presenting the system with as little as 20 percent of the information [8:348]. The amount of shift invariance is seen to be tied to the number of stored objects and their spatial widths. An increase in the memory capability of the system may be increased using nonlinear crystals as the memory element.

The major focus of this thesis is investigate the characteristics of the memory described by Owechko et al. [18]. After this characterization, a position, scale and rotation invariant version of this memory will be designed using a new feature space to represent input objects. The next chapter describes this feature space.

III. The Position, Scale, and Rotation Invariant Feature Space

3.1 Introduction

The perfect target recognition system should locate a target in its given environment. There are six major distortions of this environment which prevent the system from working [16:31]:

1. Changes in position.
2. Changes in scale.
3. Changes in in-plane rotation.
4. Changes in out-of-plane rotation.
5. Changes in physical shape.
6. Clutter.

In this thesis, a feature space that negates the effects of the first three distortions is employed for inputs and stored objects in the HAM. The last three distortions are very difficult problems and will not be dealt with in this effort.

In Chapter 1 it was mentioned the HAM is based on the classical Vander Lugt correlator. Correlation devices are inherently position invariant. The correlator will operate properly as long as the input is somewhere in the input scene and is not scaled or rotated. Casasent [2:1795] has shown scale changes of 2 percent and rotations of 3.5 degrees can cause a 27 dB drop in the SNR of the correlation peak. To extend the usefulness of the HAM to the real world environment where objects are often scaled and rotated, the $|F(f_{mr}, f_{\theta})|$ of interested objects are used as this new feature space.

3.2 The $|F(f_{lnr}, f_{\theta})|$ Feature Space

3.2.1 Introduction The ln-polar representation of the magnitude of the Fourier transform, $|F(f_{lnr}, f_{\theta})|$, has been investigated for correlation space invariance by Casasent [2], a recent AFIT graduate Mayo [16], and two present AFIT graduate students Walrond and Childress [23]. They have found the $|F(f_{lnr}, f_{\theta})|$ space is invariant in the correlation process, but the word invariant must be precisely defined. Walrond and Childress have confirmed that an autocorrelation is always present with scaled and rotated objects, however, the peak is shifted along the f_{lnr} and f_{θ} axis by an amount related to the scale and rotation difference. If the presence of an autocorrelation (not its precise location) is the required output, this space is invariant. This is the case with the holographic memory. As long as the more intense autocorrelation is present, it will be phase conjugated and returned to the hologram for reillumination.

3.2.2 Theory The theory behind each invariant part of this new feature space is now presented.

3.2.2.1 Position Invariance The position invariance is obtained by using the magnitude of the Fourier transform $|F(f_x, f_y)|$. The Fourier transform shift theorem that shows this position invariance is given by:

$$f(x \pm x_0, y \pm y_0) \xleftrightarrow{F} F(f_x, f_y) \exp^{\pm[j2\pi(x_0 f_x + y_0 f_y)]} \quad (20)$$

Equation 20 shows that shifts in the input domain become linear phase factors in the Fourier space. These phase terms do not appear when only the magnitude is kept. The $|F(f_x, f_y)|$ is the same for an object, no matter its position in the input scene.

3.2.2.2 Scale and Rotation Invariance A rotation of $f(x, y)$ causes a similar rotation in $|F(f_x, f_y)|$. Scale changes in $f(x, y)$ cause a change in the Fourier

transform given by:

$$f\left(\frac{x}{a}, \frac{y}{b}\right) \stackrel{\mathcal{F}}{\leftrightarrow} |ab|F(af_x, bf_y) \quad (21)$$

The effects of scales and rotations can be separated by performing a polar transformation on $|F(f_x, f_y)|$ yielding new spatial frequency coordinates f_r, f_θ [2:1796]. These new spatial frequencies are given as:

$$f_\theta = \arctan\left(\frac{f_x}{f_y}\right) \quad (22)$$

and

$$f_r = (f_x^2 + f_y^2)^{\frac{1}{2}} \quad (23)$$

If the two dimensional scaling is equivalent, then $(f_x/f_y) = (af_x/bf_y)$ [16:35]. The two dimensional scaling reduces to a one dimensional scale in r for the polar coordinate transform. Since rotations in space and frequency are equivalent they are now defined as linear shifts along the f_θ axis. Note that this is a cyclical shift since this shift wraps around at the right and left boundary (0 and 360 degrees).

A logarithmic scaling of the radial axis is required to accomplish the scale invariance [16:35]. Equation 21 shows that scale changes of the input, scales the magnitude of the Fourier transform as well as the spatial frequencies. Taking Equation 21 in account and scaling by a and b , Equation 23 becomes:

$$f_r = (a^2 f_x^2 + b^2 f_y^2)^{\frac{1}{2}} \quad (24)$$

Performing the natural logarithm on the above equation (assuming $a = b$) and expanding gives the scale invariant coordinate:

$$f_{\ln r} = \ln a + \ln (f_x^2 + f_y^2)^{\frac{1}{2}} \quad (25)$$

Equation 25 is a scaled (by \ln) and shifted (by $\ln a$) version of Equation 23.

An optical position, scale, and rotation invariant feature space can be generated by performing the proper coordinate transform of the magnitude of the Fourier

transform. The coordinate transform is done using a computer generated hologram (CGH) which is described in Appendix A. The ideal technique for generating the $|F(f_{lnr}, f_{\theta})|$ is shown in Figure 4.

In the ideal system, the magnitude of the Fourier transform is sensed on a Sony CCD (charge coupled device) camera. This magnitude is then displayed on a spatial light modulator (SLM) for input to the coordinate transform computer generated hologram. This result, $|F(f_{lnr}, f_{\theta})|$, is captured on another CCD camera and displayed on another SLM for input to the holographic memory.

Because two SLMs were not available for this thesis, the $|F(f_x, f_y)|$ is captured on Polaroid High Contrast (HC-135-12) instant film. These slides were used as inputs to the coordinate transform (CT) CGH. The $|F(f_{lnr}, f_{\theta})|$ was then photographed. The $|F(f_{lnr}, f_{\theta})|$ version of the objects were transferred to glass slides for use in the memory by placing the 35mm and glass slides together in the Dekacon camera system described in Appendix A to make a 1 to 1 negative. The result is a clear glass slide with dark information areas. The slides used for this research were generated with the help of Walrond and Childress [23]. The images obtained from their experimental apparatus were of much higher quality than those I could make since it was dedicated to the precise production of the $|F(f_{lnr}, f_{\theta})|$. Photographs of the original objects, their Fourier transforms, and the $|F(f_{lnr}, f_{\theta})|$ representation are found in Appendix B. The thesis of Walrond and Childress should be seen for further reference on the PSRI feature space [23].

The next chapter describes an important element of the holographic associative memory, the phase conjugate mirror. The operational theory is discussed and the characteristics of the mirror are presented.

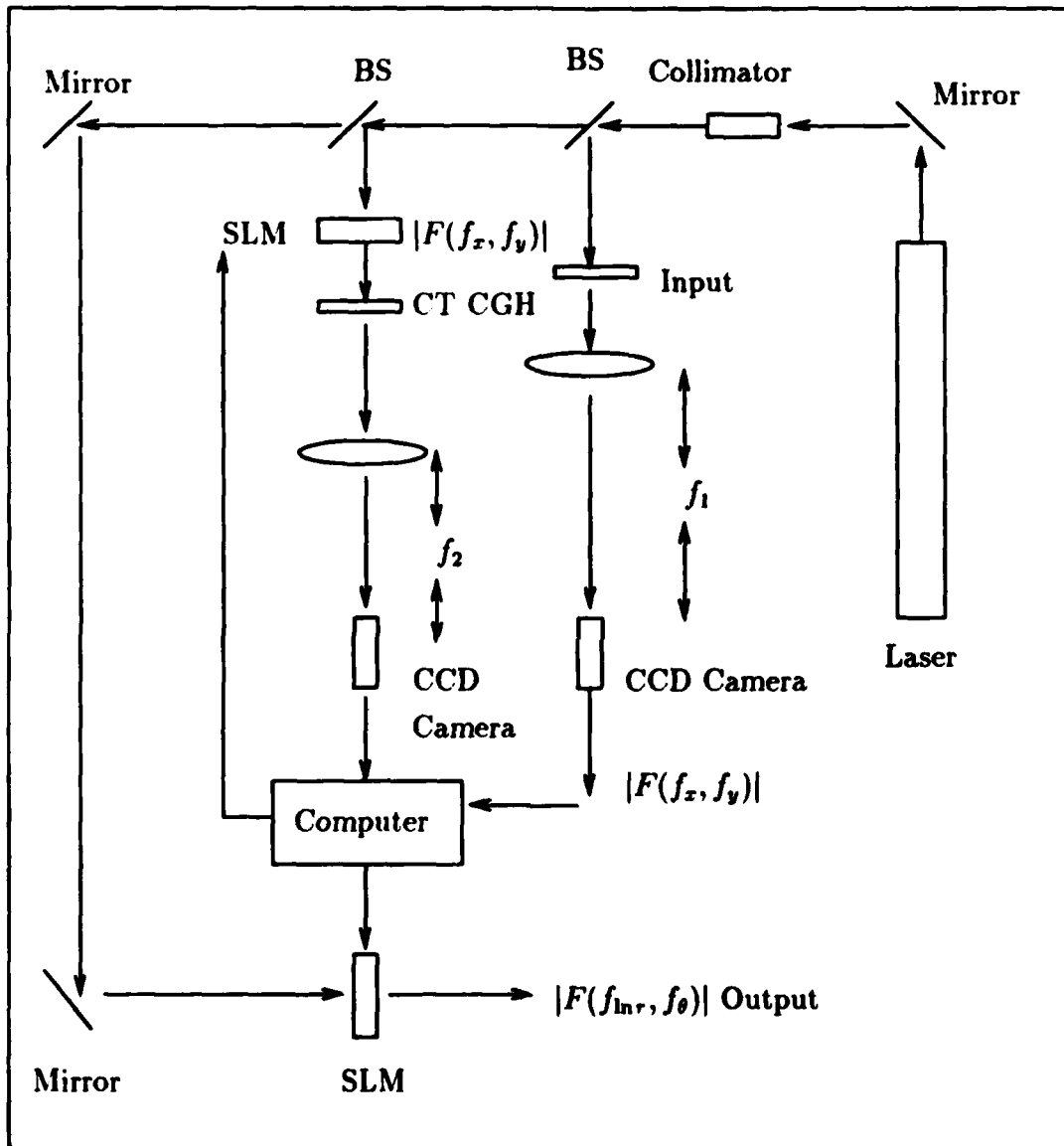


Figure 4. $|F(f_{inr}, f_{\theta})|$ Generation Method.

IV. The Phase Conjugate Mirror

4.1 Introduction

The phase conjugate mirror is perhaps the most important element in the holographic associative memory. The PCMs nonlinear thresholding property is responsible for selectively conjugating the strongest correlation reference produced by the hologram. These beams compete to build their own photorefractive grating to produce a phase conjugate beam. Only the strongest correlation, the autocorrelation, will build the grating and produce a phase conjugate return while suppressing all other possible cross-correlation returns.

The phase conjugator used in this thesis is a single domain crystal of $BaTiO_3$. Single domain implies the crystal's lattice structure is uniform for the entire volume. The crystal measures 5mm by 5mm by 3mm with the c-axis parallel to a 5mm edge. One of the major objectives of this thesis is to characterize the phase conjugate reflectivity of the $BaTiO_3$ through self-pumped phase conjugation. With the crystal in air at room temperature, the cw phase conjugate reflectivity vs incident beam angle is measured using an argon-ion laser operating in a single longitudinal mode (with internal étalon) at 488.0nm.

4.2 Background

The operational theory of the self-pumped conjugator has been described in detail by MacDonald and Feinberg [14:549-550]. They have shown the device uses four-wave mixing in two coupled interaction regions, extending the case of one interaction region presented by Cronin-Golomb et al. [6]. In the crystal itself, there are two counter-propagating beams that mix by the photorefractive effect producing the phase conjugate return. The internal beam structure for the two interaction regions is shown in Figure 5 [9:487].

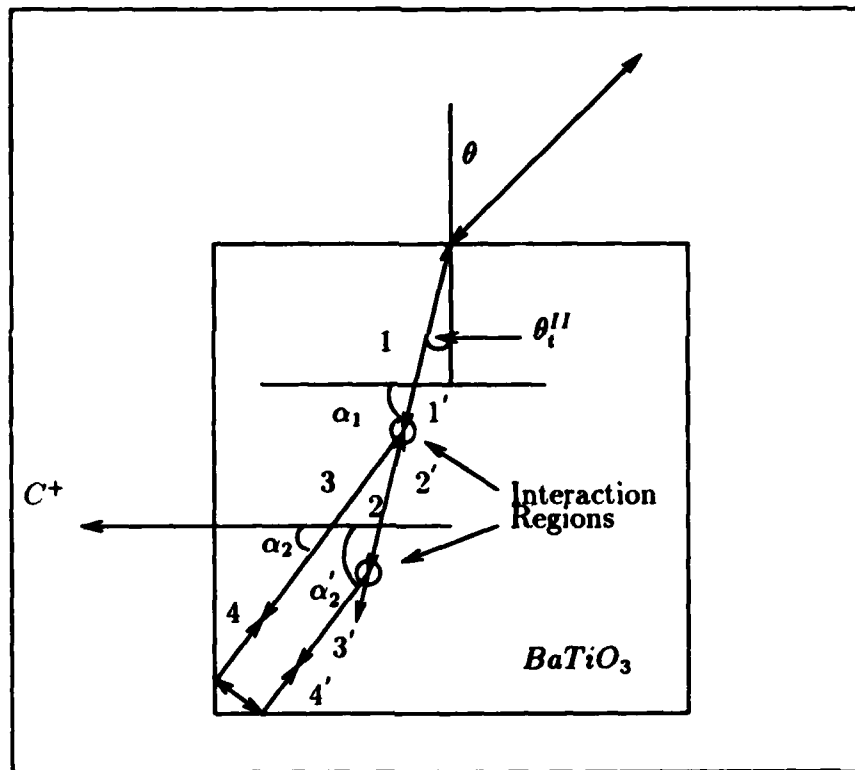


Figure 5. Phase Conjugate Beam Path.

There are four beams in each interaction region; an input beam, the phase conjugate return, and two pumping beams. Beams (1, 3, and 4) contribute to form 1' and (2, 3', and 4') to form 2' which combine to make the total phase conjugate return. If the internal angles α_2 and α_2' are not equal, the PCM still operates but 2' and 1' will be of different strengths. Two justifications are considered for the presence of the two coupled regions. First was photographic evidence given by Feinberg [9:487] clearly showing the beam paths inside the crystal matched those from theory seen in Figure 5. Second is that two interaction regions provide freedom for the pumping beams to adjust their paths maximizing the phase conjugate reflectivity. For one interaction region this freedom to adjust paths does not exist.

4.3 Coupling Strength

The solutions to Maxwell's equations of the four electric fields in the two interaction regions is summarized in reference [14:551-552]. The important concept to be carried forward is the role of the crystal characteristics and beam geometry on the phase conjugate return. The photorefractive effect, due to the first order nonlinear polarization, is the mechanism where charge migration due to varied light intensity patterns produce a change in the refractive index of the material. The resulting magnitude of the charge density pattern, or grating, and its diffraction efficiency depend on the Pockels coefficients of the material, the angle of the optical beam with the material's c-axis, and the density of charge carriers in the material. This magnitude is related to the coupling strength, γl , between the input beam and its phase conjugate return. γ is the coupling strength per unit length and l is the length of the material. Fisher et al. explains the origin of the coupling strength in reference [10]. Cronin-Golomb [5:691] describes the properties of the coupling strength as:

When it is real, the phase shift between the light interference pattern and the refractive index grating is $\pi/2$. This is a behavior typical of photorefractive materials with no bias field. When γl is purely imaginary, the index grating is in phase with the light interference pattern, which is the case in media which have a local response such as atomic vapors.

In the case of the self-pumped phase conjugator, the coupling strength is real and causes a $\pi/2$ phase shift in the incident beam. The following treatment of the coupling strength follows that given by Feinberg[9]. The cw steady state coupling strength per unit length given by:

$$\gamma = \frac{\omega r_{\text{eff}} E}{2nc \cos\left(\frac{\alpha_1 - \alpha_2}{2}\right)} \quad (26)$$

E has units of electric field. When not in the presence of an applied or intrinsic dc electric field E has the form:

$$E = \frac{k_B T k_g \hat{e}_1 \cdot \hat{e}_2^*}{q \left(1 + \left(\frac{k_g}{k_0}\right)^2\right)} \quad (27)$$

Where k_o is determined by the charge density N given by:

$$k_o = \left(\frac{Nq^2}{\epsilon\epsilon_o k_B T} \right)^{1/2} \quad (28)$$

Here \hat{e}_1 and \hat{e}_2 are two beams with unit polarizations, α_1 and α_2 are internal angles shown in Figure 5, ω is the optical frequency, $k_B T$ is the thermal energy, q is the charge of the carriers, $k_g = 2(n\omega/c) \sin(\alpha_1 - \alpha_2/2)$ is the signed magnitude of the grating wave vector k_g , ϵ_o is the permittivity of free space, and ϵ is the dielectric constant. For crystals of point group 4mm the effective Pockels coefficient, r_{eff} , is given by:

$$r_{eff} = n_o^4 r_{13} \sin \left(\frac{\alpha_1 + \alpha_2}{2} \right) \quad (29)$$

for ordinary polarized light (perpendicular to the c -axis) and

$$r_{eff} = \left[n_o^4 r_{13} \cos \alpha_1 \cos \alpha_2 + 2n_e^2 n_o^2 r_{42} \cos^2 \left(\frac{\alpha_1 + \alpha_2}{2} \right) + n_e^4 r_{33} \sin \alpha_1 \sin \alpha_2 \right] \sin \left(\frac{\alpha_1 + \alpha_2}{2} \right) \quad (30)$$

for extraordinary polarized light (parallel to the c -axis). n_o and n_e are ordinary and extraordinary indices of refraction at ω and r_{ij} are elements of the electro-optic tensor.

For $BaTiO_3$, values for these constants are $n_o = 2.517$ and $n_e = 2.505$ at 488.0nm. The components of the electro-optic tensor are $r_{13} = 8$, $r_{33} = 28$, $r_{42} = r_{51} = 820$ given in units of $10^{-12}m/V$. The typical charge density is $N = 2 \times 10^{16}cm^{-3}$ and the relative permittivity is $\epsilon_{||} = 106$ and $\epsilon_{\perp} = 4300$.

These values are substituted into Equation 26 to determine how the coupling strength depends on the internal angle α_1 . The angle α_2 was assumed to be 6 degrees less than α_1 for most angles as noted by Feinberg [9:487] and the incident polarization is extraordinary to access the higher effective Pockels coefficient. The plot of the coupling constant is shown in Figure 6.

Figure 6 shows the interior angle, α_1 , for maximum coupling and phase conjugate reflectivity is about 40 degrees. Since $BaTiO_3$ is negative uniaxial crystal,

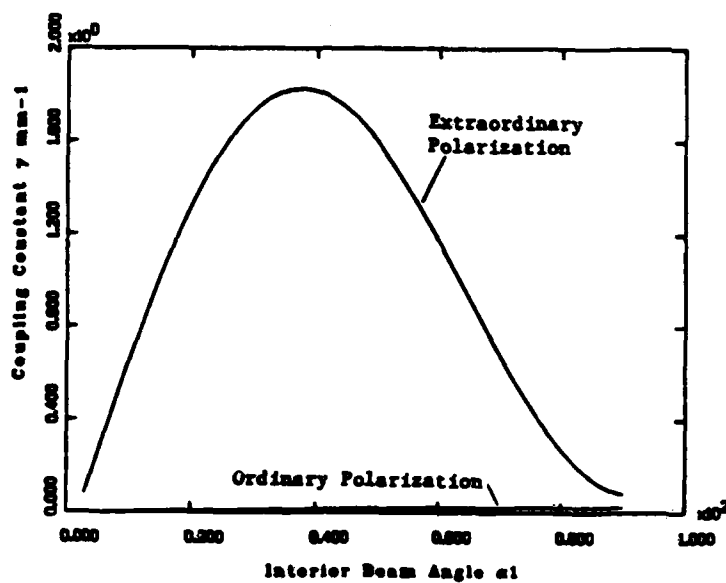


Figure 6. Coupling constant per millimeter versus interior beam angle α_1 .

the extraordinary polarized index of refraction, n^{II} , is dependent on the angle of incidence θ , and is determined by the following equation:

$$n^{II} = \left(n_e^2 - \left[1 - \left[\frac{n_e}{n_o} \right]^2 \right] \sin^2 \theta \right)^{\frac{1}{2}} \quad (31)$$

This value is used to determine the interior beam angle with the crystal normal which is given by Snell's Law:

$$\theta_i^{II} = \arcsin \left(\frac{\sin \theta}{n^{II}} \right) \quad (32)$$

From the geometry shown in Figure 5, the interior angle α_1 is $90 - \theta_i^{II}$. Several values of θ , are substituted into Equation 31 and the resulting θ_i^{II} s into Equation 32, and the possible interior angles are shown in Table 1.

This table shows that with the crystal in air, the maximum attainable value of the coupling constant, γ , is when the input beam is incident at 90 degrees. As the input angle θ is increased from 0 degrees, α_1 increases along the backside of the curve

θ	θ_t''	α_1
0.0	0.00	90.00
10.0	3.98	86.03
20.0	7.85	82.15
30.0	11.52	78.48
40.0	14.87	75.13
50.0	17.82	72.19
60.0	20.24	69.76
70.0	22.05	67.95
80.0	23.17	66.83
90.0	24.54	66.46

Table 1. Incident Angle, Transmitted Angle and the Angle with the Crystal c-axis.

shown in Figure 6. Index matching fluids or a 45 degree cut crystal are needed to access the greater coupling constant. MacDonald and Feinberg [14:552] have shown that a coupling strength of $\gamma l = 2.34$ is required to initiate the phase conjugation process. For typical incident angles of 60 to 70 degrees the coupling constant, γ , is between 1.1 and 0.7 . These values of γ combined with propagation length $> 5\text{mm}$, assure a phase conjugate return.

4.4 The Experiment

The measurement of phase conjugate reflectivity was performed using the experimental setup shown in Figure 7.

The power in the collimated beam before the beamsplitter is 27.9 mW. The power of the beam passing through is 22.7 mW with 5.0 mW reaching the crystal. The crystal is placed on a rotation base, designed during this research, so the input angle can be varied. The extraordinary beam orientation is found by maximizing the phase conjugate return for several angles while adjusting the polarization rotator of the laser. The exact positioning of the crystal in relation to the focal plane of the lens is somewhat arbitrary. Some defocusing to give a beam diameter of $\approx 1\text{mm}$

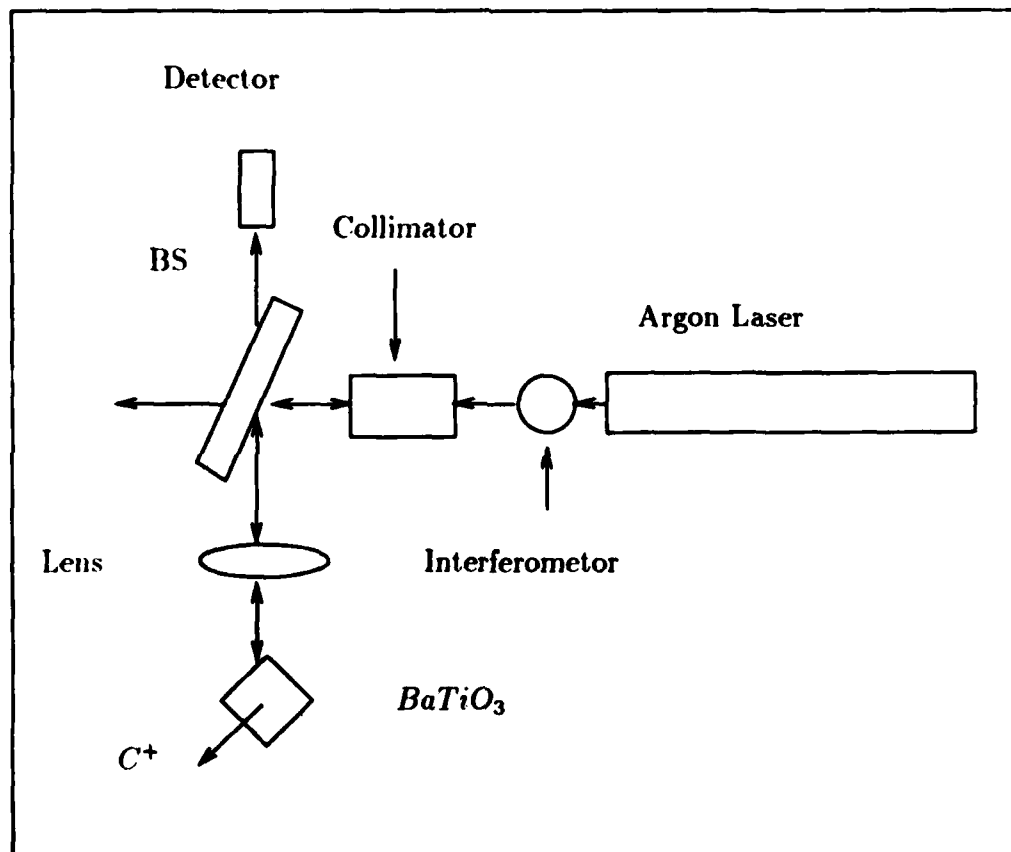


Figure 7. PCM Reflectivity Experiment.

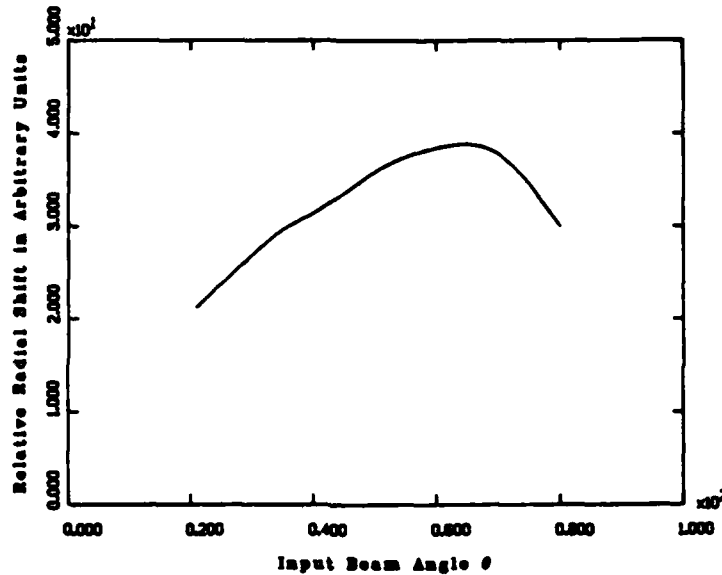


Figure 8. Phase Conjugate Reflectivity.

gave the best conjugate returns. At angles greater than 70 degrees, the crystal was moved in relation to the lens to maintain the 1mm beam diameter.

To measure the phase conjugate return for a given angle, the beam is aligned in the crystal at that angle. The crystal is then rotated at least 10 degrees to destroy any grating that may have built up during alignment. The beam is blocked and the crystal rotated back to the proper angle. The beam is unblocked and an X-Y recorder connected to the detector is started. The phase conjugate reflection is measured every 5 degrees from input angles of 0 to 90 degrees.

4.4.1 Experimental Results The results of the phase conjugate reflectivity experiments are shown in Figure 8. For angles below 20 degrees, no phase conjugate return was seen. From 30 degrees to 60 degrees a steady increase is seen in the return maximizing at 38.5% not accounting for Fresnel loss. Fresnel loss is the light reflected off the face of the crystal that does not take part in the phase conjugation process. After 60 degrees, the return begins to decrease. This is partly attributable to more power being reflected off the front crystal face, leaving a smaller fraction of beam available for phase conjugation. A photograph of the device while phase conjugating

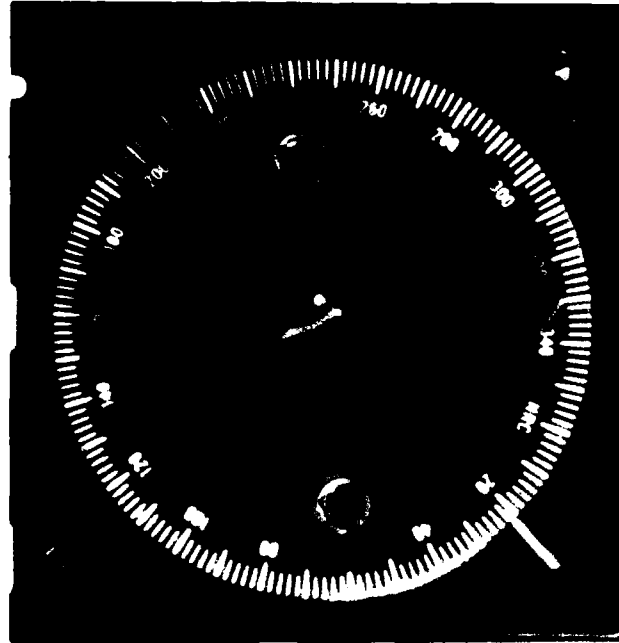


Figure 9. Photograph of the PCM While Phase Conjugating. The Beam Enters from the Right.

is seen in Figure 9. Wilson reports a maximum phase conjugate reflectivity of 50% with a 45 degree cut crystal measuring 5mm by 5mm by 5mm [24].

The buildup of the phase conjugate return was dependent on the incident angle θ . For angles between 30 and 80 degrees, the phase conjugate signal would appear in ≈ 10 seconds, with the time response increasing slightly with increasing angle, abruptly build to $\approx 90\%$ of its maximum value in 2-3 seconds, and slowly increase to its maximum value in 1 minute. For angles between 22 and 30 degrees there is a smaller return that behaved somewhat erratically, taking up to 2 minutes to build up to maximum return and continuing to vary by $\pm 10\%$. For angles between 20 and 22 degrees, the phase conjugate output went into a periodic oscillation with a low return. This result was totally unexpected. A further literature search uncovered several articles describing this periodic behavior. Among these are papers by Smout and Eason [19] and Kwong and Yariv [13]. They describe possible mechanisms causing this effect as the self-pumping changing channels and a beating of the two

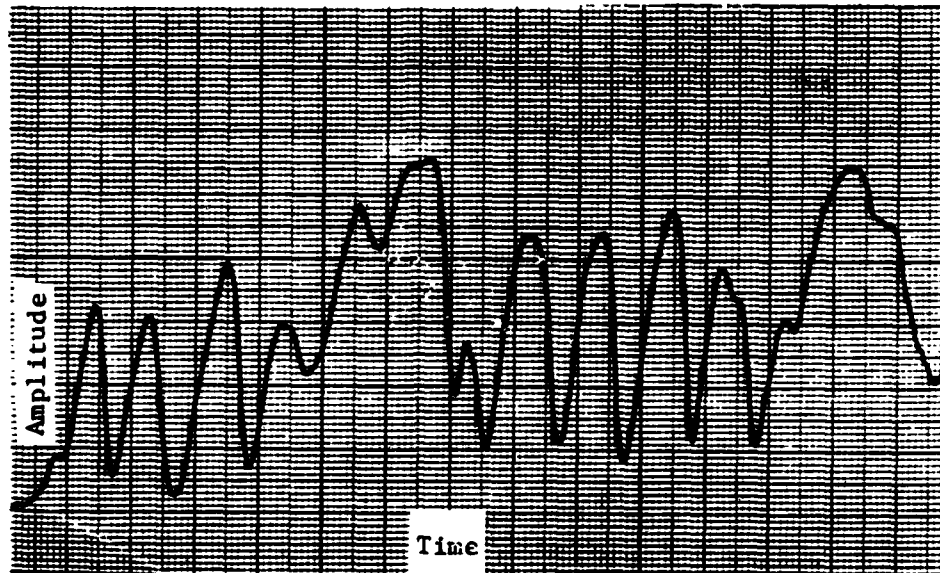


Figure 10. Phase Conjugate Oscillation.

phase conjugate beams internal to the crystal. They also describe this oscillation for incident beams that strike the crystal high on the face opposite the corner reflector. A graph of this oscillation is seen in Figure 10.

4.4.1.1 Aberration and Resolution Measurements A scratched glass plate was placed in the beam just after the beamsplitter to demonstrate that the phase conjugate process negates the effect of aberrations. With the crystal producing the phase conjugate signal, the plate was placed into the beam. The signal disappeared and reformed in approximately 10 seconds.

To measure the resolution of the conjugate return, a glass slide of the U.S. Air Force resolution chart was inserted before the beam splitter shown in Figure 7. The smallest clearly identifiable lines from the chart came from group 3, element 6. The resolution of group 3, element 6 corresponds to 14.25 lines/mm. Note the difference

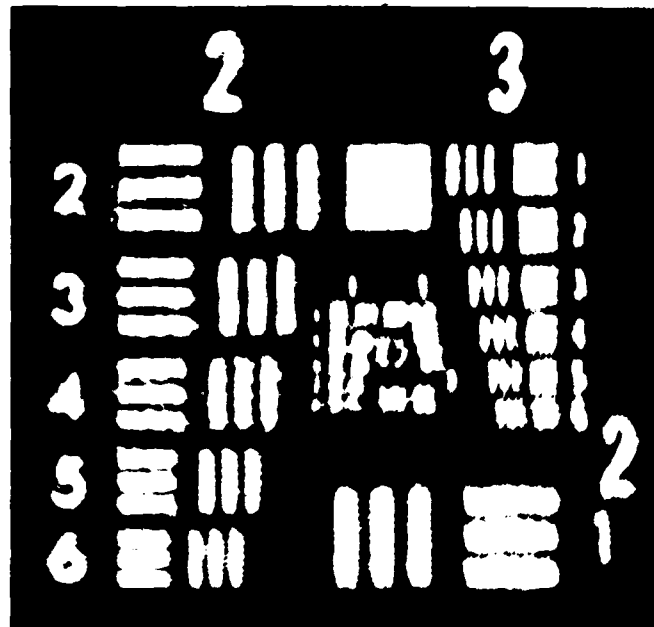


Figure 11. Phase Conjugate Return of the Resolution Chart.

in resolution for the horizontal and vertical bars. This is because the higher spatial frequencies required to reform the smaller bars are lost in one direction since the dimensions of the incident face is 5mm by 3mm. A 17cm lens is used to focus the input beam onto the crystal. Using a shorter focal length lens will improve the resolution capability of the PCM. This resolution was observed with and without an aberrator in the incident beam. A photograph of the phaseconjugated resolution chart is show in Figure 11.

Owechko et al. reported 16 line pairs/mm for the self-pumped conjugator and 128 line pairs/mm for DFWM [18:1909]. Wilson reports a resolution of 156 lines/mm with the z-cut crystal used in this thesis under the conditions of two-wave mixing image amplification [24]. The resolution chart was imaged onto the crystal with a reduction of 5. The minimum resolution is from group 5, element 1 yielding 32 lines/mm and extrapolating the reduction of 5 gives the 160 lines/mm.

4.5 Summary

The phase conjugate reflectivity experiments have shown the crystal will produce a return $> 30\%$ over a 40 degree range (40 to 80 degrees) and $> 35\%$ over a 20 degree range (50 to 70 degrees). The phase conjugate return is very robust, in that it is self-aligning. Within limits of beam diameter, a return is easily seen by sending the beam toward the corner of crystal. The crystal demonstrated its ability to cancel distortions placed in the beam. Image bearing beams were returned with a resolution of 14.25 lines/mm.

The amount of reflected energy in the phase conjugate return is very important for system operation. As much energy as possible must be returned to the hologram for reillumination. The diffraction efficiency of the hologram itself plays a major role on how much light passes in the first diffracted order and is returned in the zero order upon reillumination. The next chapter discusses the other important element of the HAM, the angle multiplexed hologram.

V. *The Hologram*

5.1 *Introduction*

The method of wavefront reconstruction or holography was invented by Dennis Gabor in 1948. The basic idea is that two coherent waves could be interfered and amplitude and phase of this interference pattern recorded. Illumination of this recording with either original wave reconstructs the other. In the early 1960's Leith and Upatnieks first described holography with optical frequencies using the newly invented laser as the long sought source of coherent light and high resolution photographic plates as a recording medium. Many methods of storage and recall of wavefronts were discovered. The off-axis transmission hologram described by Leith and Upatnieks in 1962 is the variety of hologram used in the holographic associative memory.

The theory for recording the off-axis Fourier transform holograms used in the memory was presented in Chapter 2. This chapter describes the characterization of the recording plates and the recording and development methods used. The holograms were bleached to produce phase holograms yielding the higher diffraction efficiencies required for the memory to operate.

The laser used in this thesis is a Spectra Physics Model 2020-3. The laser is operated in a single longitudinal mode (with étalon) at 488.0nm. The laser is 99.8 percent polarized and has a polarization rotator on the output coupler.

5.2 *The Holographic Plates*

The holographic recording material used at the beginning of this thesis was the 4" x 5" 10E56 holographic glass plates made by the Agfa-Geavert Corporation. These plates are sensitive for wavelengths from 350nm to 575nm. The energy per unit area that corresponds to a transmittance of 0.5 is $\approx 1\mu\text{J}/\text{cm}^2$ for 488.0nm.

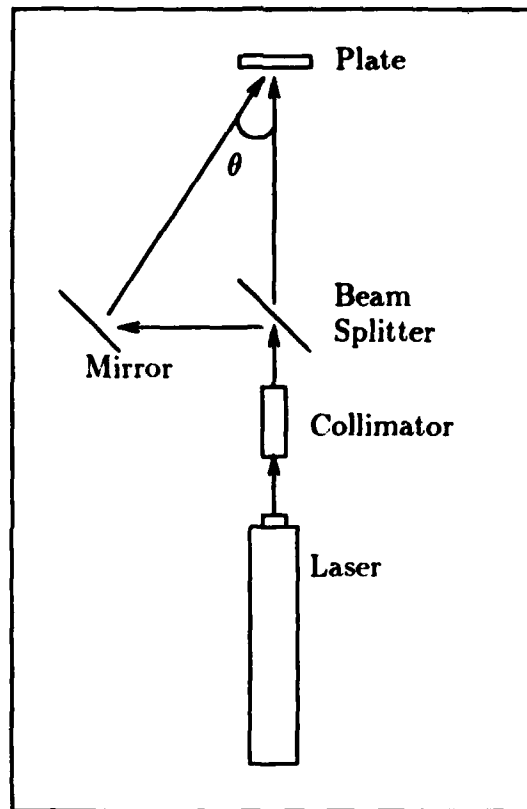


Figure 12. Recording of Plane Waves.

To characterize the exposure times and development process for the optimum diffraction efficiency, two plane waves were recorded on the plates using the configuration shown in Figure 12.

For this experiment, the collimated beam is divided with a beamsplitter and the energy in each beam is equal at $0.050mW/cm^2$. Since the total energy on the holographic plate is $0.1mW/cm^2$ the exposure time to achieve a transmittance of 0.5 is 10 msec. An electronic shutter is used to regulate exposure times. The angle between the reference and main beam is 20 degrees. The development process used for producing phase holograms is recommended by Collier [3:290]:

1. Develop in D-19 5 minutes.

2. Rinse for 1 minute.
3. Fix in Kodak Rapid Fixer 5 minutes.
4. Rinse 2 minutes.
5. Bleach 3 minutes in 5 percent solution of Potassium Ferricyanide.
6. Rinse 5 minutes.

The first holograms developed were amplitude holograms, made by deleting the bleaching step. Plates were made with exposure times of 10msec through 100msec in steps of 10msec. All plates had a diffraction efficiency of between 0.25 and 2 percent. A set of plates with similar exposure times were made and bleached. All plates had a diffraction efficiency in the same region except one plate exposed at 20 msec which had a diffraction efficiency of 11 percent.

The typical amplitude hologram has a maximum theoretical diffraction efficiency of 6.25 percent with efficiencies of 4 to 5 percent typical [3:261]. Bleached holograms can theoretically achieve 100 percent diffraction. The manufacturer states the bleached efficiency of the 10E56 plates is approximately 30 percent. It was felt an adjustment needed to be made in the exposure times, based on the average exposure energy, and development process to bring the amplitude holograms consistently up to the 4 to 5 percent diffraction efficiency range. Many ranges of beam energies, exposure times, and development times were used. After approximately 50 more unbleached holographic plates were exposed, none had a diffraction efficiency above 2 percent. Another 50 plates were exposed with some bleached. Midway in this round of exposures, the bleach was changed to a formula recommended by Hariharan and Chidley [11:3066]. They reported diffraction efficiencies up to 70 percent with their method. The bleaching solution is:

1. Bleach time: 8 minutes.
2. 0.8 gm of Potassium Dichromate.

3. 1 ml of Sulfuric Acid.

4. deionized (DI) water to a liter.

With this mixture, they recommend not fixing the plate, but no difference was obtained with fixed or unfixed plates. The results of this round of testing did not produce a plate, bleached or not, with a diffraction efficiency above 2 percent. At this point, the inability to create a hologram put the development of the holographic memory in serious jeopardy. A sample of the developed and unexposed plates were sent to the Agfa-Geavert Company for testing at their request. No results were reported at this writing.

5.3 *The Kodak HRP 1-A Plates*

The team of Walrond and Childress and myself had recently received an order of Kodak 1-A high resolution plates (HRP) that were used to create the computer generated hologram used in the coordinate transform and to make the original transparencies of our objects. These plates were sensitive to blue-green wavelengths. After some investigation, it was found the wavelength sensitivity was from 420nm to 570nm. The resolution of the plates is 2000 lines/mm, acceptable for holography. A company brochure described the *H&D* curves for the plates under various concentration of developer and development time. The next step was to experimentally determine if a hologram could be made in the material and determine the transmittance vs. exposure, *t-E*, curve of the film.

There are several variables involved in producing an amplitude transmission hologram. These include exposure time, development time, beam energies, and beam angles. If any of these are changed, the transmittance of the recording will change. For consistency, the following recipe for the development of the plates were used and never deviated from. This process is:

1. Develop in D-19 for 2 minutes

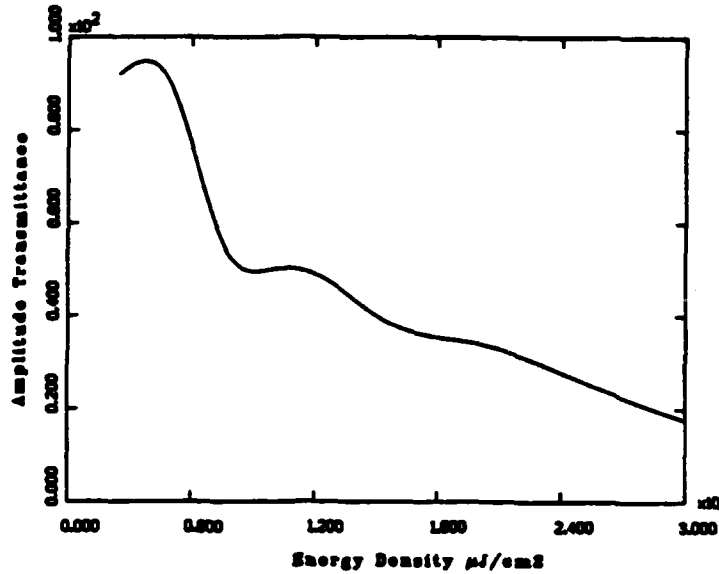


Figure 13. t-E Curve for Kodak 1-A Plates.

2. Rinse 1 minute
3. Fix in Kodak Rapid Fixer 1 minute
4. Rinse 5 minute

Beam powers were chosen to be $.25\text{mW}/\text{cm}^2$ and exposure times ranged from 5msec to 60msec in steps of 5msec. These exposure times equate to beam energies per unit area of 2.5 to $30\mu\text{J}/\text{cm}^2$. The angle between beams for all exposures is 20 degrees. The transmittance function produced is seen in Figure 13. All plates had a diffraction efficiency between 3.2 and 4.7 percent which is in the expected range for a good amplitude transmission hologram. Exposure times between 10 and 15msec yielded a transmittance of approximately 0.5. Several plates were exposed at 1, 3, and 5 times this average exposure and bleached in the previous bleaching solution. No increase in diffraction efficiency was noted. Since the amplitude holograms gave good diffraction efficiencies, the bleach was assumed to be defective.

Hariharan and Chidley reported using a conventional bleach with potassium bromide included in the previous recipe [11:3066]. Bleaching in this solution immediately produced plates with a higher diffraction efficiency. A curve of diffraction

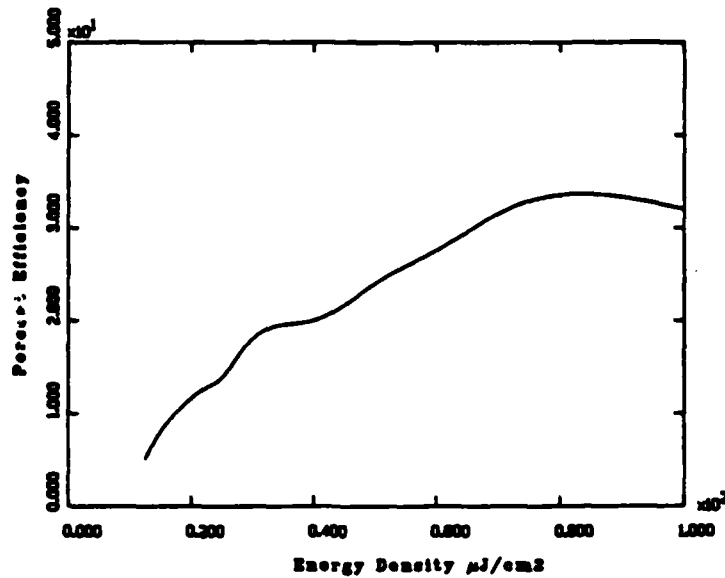


Figure 14. Diffraction Efficiency of Bleached Holograms.

efficiency vs beam energy per unit area is seen in Figure 14. The maximum diffraction efficiency was 32 percent. The final development procedure used to make all bleached holograms is:

1. Develop in Kodak D-19 for 2 minutes.
2. Rinse 1 minute.
3. Fix in Kodak Rapid Fixer 1 minute.
4. Rinse 1 minute.
5. Bleach 8 minutes.
 - 0.8 gm of Potassium Dichromate.
 - 4.0 gm of Potassium Bromide.
 - 1 ml of Sulfuric Acid.
 - DI water to 1 liter.
6. Rinse 5 minutes.
7. Place in Kodak Photo-Flo 1 minute.

8. Air Dry

When reconstructing the plane wave hologram, multiple reproductions of the off-axis reference beam were produced. This is due to the multiple reflections from the front and rear of the beamsplitter in the recording and reillumination process. Beamsplitting and separately collimating the main object beam and reference eliminated this multiple output and increased the diffraction efficiency to 37 percent.

5.4 Summary

The making of the hologram was assumed to be one of the least involved aspects of this thesis. It turned out to be the most involved, taking approximately 1 month of experimentation to produce reliable, high diffraction efficiency holograms. Holograms of plane waves can be consistently made with up to 37 percent diffraction efficiency by collimating each beam separately. Now that the technique for producing these holograms is understood, the holograms for the memory can be made. The next chapter describes the construction of the memory and the experimental results.

VI. The Experiment

6.1 Introduction

Now that the phase conjugate mirror has been characterized and the holographic development process is understood, the holographic associative memory can be constructed. The experimentation with the memory will fall into the areas described in the thesis approach in chapter 1. The major area is to redemonstrate the experiments reported by Owechko et al. [18]. Operating parameters of the system such as the amount of allowable shift and rotation of inputs will be investigated.

6.2 The Design

The type of hologram used in the holographic memory is the Fourier transform hologram. The experimental setup is similar to that of the off-axis recording of plane waves in the previous chapter except the object and Fourier transform lens are introduced. The configuration is shown in Figure 15.

The beam emitted from the laser is divided by a beam sampler. The beam sampler directed approximately 1 percent of the energy toward the collimator for the off-axis reference beam. The beam sampler was chosen over a traditional beam splitter so more energy would be available for reconstruction with the main object beam without having to realign the optics if a beam splitter were used and removed. Each beam is separately collimated to avoid recording the multiple reflections noted in the previous chapter. The collimator for the reference beam was a 20x objective, a 15 μ m pinhole, and an 17.8cm focal length lens. This combination of pinhole and objective gave a fairly uniform reference beam. The reference was apertured to approximately 4.0cm to expose as much of the holographic plate as possible. The collimator for the main beam consisted of a 10x objective, a 25 μ m pinhole, and a 17cm JODON telescopic collimating lens. The main beam diameter was

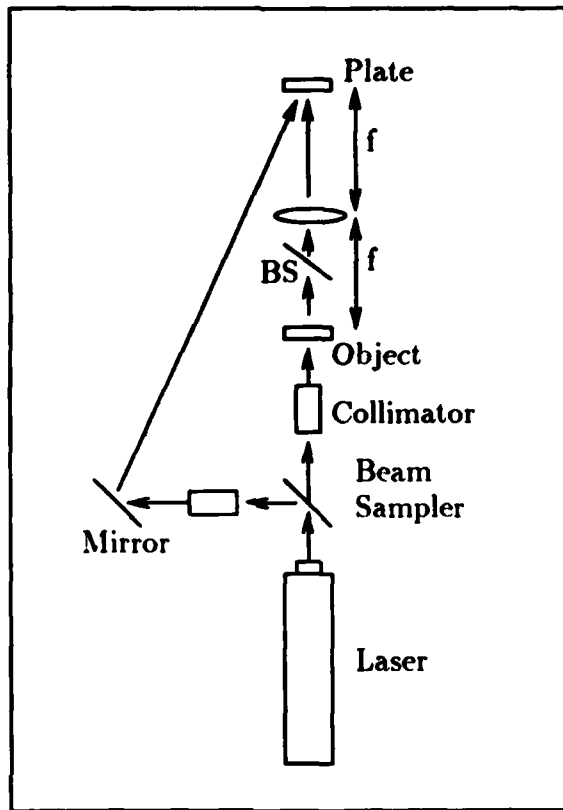


Figure 15. Hologram Recording Method for the HAM.

approximately 1.5cm in diameter with no aperture. This small beam diameter was chosen so more energy would be scattered in the forward direction toward the lens.

The Fourier transform lens focal length is 17.8cm. A 3in beamsplitter is placed near the lens to couple the output of the memory to the output plane. The front focal plane of the lens was determined by measurement and the input object slide holder was secured at this location. A card was placed in the holographic plate holder and placed in the back focal plane by measurement. A glass slide of a small square was placed in the input holder and illuminated. The back focal plane was accurately determined by adjusting the plate holder until the 2-dimensional Sinc pattern of the Fourier transform of the square was in clear view. The input slide could be moved with no apparent movement of the 2-dimensional Sinc. This was

could be moved with no apparent movement of the 2-dimensional Sinc. This was convincing evidence the input slide is in the front focal plane and the holographic plate holder was in the back focal plane of the lens.

6.2.1 Exposure of the Holographic Plates With the optical system properly aligned, the holograms are now ready to be made. A 2" x 2" ground glass diffuser is taped in contact with the glass slide of a opaque triangle on a clear background. The ground glass is made by sandblasting one side of a sheet of plate glass. The diffuser has two important properties. First, the diffuser spreads out the energy in the Fourier transform so a more linear recording can be made. Upon reconstruction, a reference beam of the same size used at exposure will travel toward the PCM instead of a diffracted version of the transform itself. This allows much more energy to reach the PCM and be phase conjugated toward the hologram for reconstruction and output. Secondly, each point on the diffuser acts as a point source enhancing the autocorrelation function compared to cross-correlations [18]. One drawback to the diffuser is if the input object and diffuser are moved relative to one another after exposure, the original object will not reconstruct as this movement effectively creates a new and different object.

The beam energies chosen for exposure are $0.5mW/cm^2$ in the reference beam and $0.050mW/cm^2$ in the main object beam. The 10 to 1 ratio yielded a higher diffraction efficiency by ensuring a linear recording [3:163]. Exposures were made for times of 40msec to 240msec at 10msec intervals.

6.3 Experimental Results

The relative diffraction efficiency of each plate was determined by illuminating the plate with the reference beam and measuring the energy in the first diffracted order. The plate exposed at 240msec has a relative diffraction efficiency of 15 percent. This developed plate is replaced in the system shown in Figure 16.

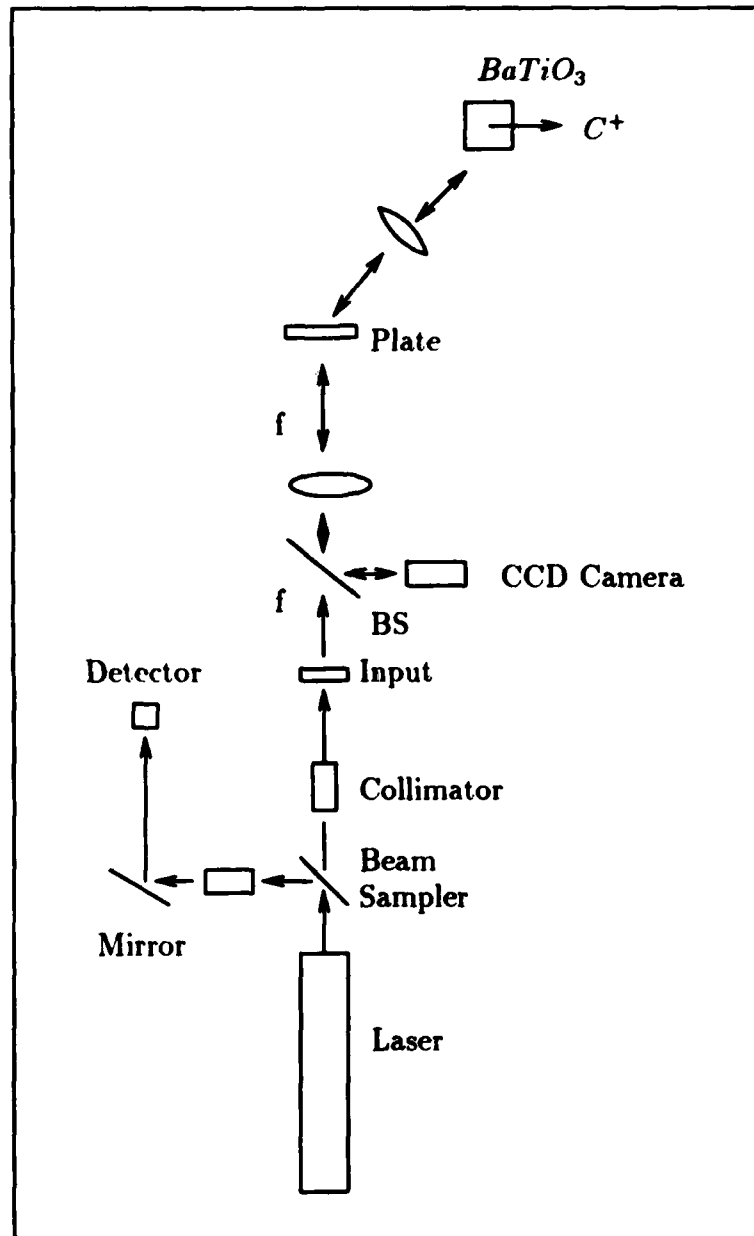


Figure 16. The Holographic Associative Memory.

The holographic plate holder is held on a rotation base mounted to a 3-axis positioner. The hologram had to be replaced within $15\mu\text{m}$ of its original position to satisfy the requirements of reconstruction [18:1909]. Replacing the hologram exactly was a tedious process which could take up to 10 minutes. When the hologram is reinserted in the holder, a diffuse beam of light is seen in the first diffracted order. If the plate is moved slowly from side to side, a position will be found where the area where the reconstructed reference should be will darken and a portion of the is area will be extremely intense. Adjustment of the rotation base and x-y positioners fill out the entire reference. The vertical positioner was too sensitive to be used for adjustment.

With the intense reconstructed reference present, a transforming lens and the PCM are placed in the beam. The optimum incident angle on the PCM of 60 degrees was chosen from the PCM experiments. The internal beam diameter in the crystal was approximately 1mm, chosen from the same experiments. Because of low beam intensity on the crystal, the phase conjugate output took approximately 2 minutes to build. The output was recorded on the Sony CCD camera. The original object and its associative output are seen in Figure 17.

6.3.1 Shift Invariance Experiment To demonstrate the shift invariance of the HAM, slight pressure was applied to the post holding the input transparency and diffuser. The slightest pressure caused the reconstructed reference beam to fade. Lateral movement of the slide in the holder caused the reference to disappear as well. This result was very disturbing. The reason for using Fourier transform holograms was to circumvent the stringent position requirements of the Fresnel hologram.

Dr. Mills, a member of my thesis committee, suggested imaging the Fourier transform to see the results when the input object was moved. The transform was imaged approximately 20 feet from the holographic plate holder using an 11.5cm lens and mirror to direct the transform toward a wall. A transparency of a clear triangle

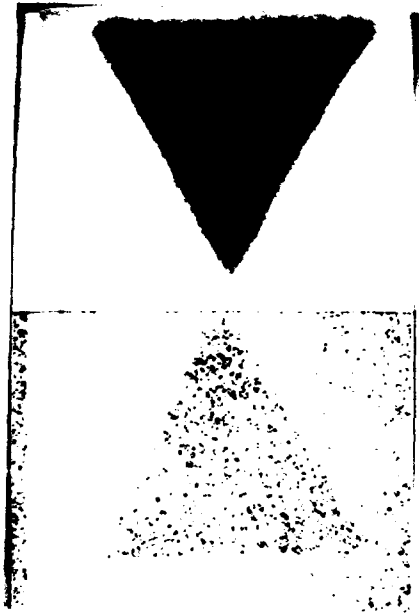


Figure 17. The Triangle (above) and its Associative Output (below). The Inversion is Due to Imaging the Original Object onto the CCD Camera.

on black background was placed in the input slide holder and its Fourier transform was clearly seen. Moving the input transparency from side to side in the object beam produced no movement in the Fourier transform as expected. The dark triangle on clear background and diffuser was placed in the input holder. The diffuse speckle pattern was observed in the output. Movement of the input slide mount caused movement in the speckle pattern.

6.3.1.1 Reasons for the Shift Problem The effect of losing the shift invariant property must be due to the characteristics of the diffuser, the relatively large $f/\text{No.}$ of the lens (3.5), or a combination of the two. The lens diameter is 50.4mm.

In a telephone conversation before this experiment, Dunning informed me he had made a characterization study of phase diffusers used in their holographic associative memory [7]. Dunning noted that the ground glass diffuser used in this thesis should work but recommended studying diffuser properties to improve the system performance.

The reason for losing the shift invariant property of the input is all of the energy leaving the object diffuser is not being captured by the optic. When placing a screen near the lens only 25 percent of the diffuse illumination enters the optic. This measurement is made on the diameter of 10 percent of the maximum power in the diffuse spot, which is 4in compared to the 2in optic. Therefore, when the input object is shifted, a "different" object is seen by the lens and the requirements for reconstructing the Fourier hologram are not met. To alleviate this constraint, a large diameter lens can be used and/or an artificial diffuser developed so all the illumination from the object enters the lens.

6.3.2 Artificial Diffusers A literature review of artificial phase diffusers used in conjunction with Fourier transform holograms produced two interesting papers by Iwamoto [12] and Nakayama and Kato [17]. Iwamoto describes the major drawbacks of Fourier transform holography as [12:215]:

1. As spectral image components are unevenly distributed, image details, which disperse weakly at high frequencies, can hardly be recorded and reconstructed (narrow bandwidth).
2. Strong low frequency image components saturate the recording media generating nonlinear noises, which make reconstructed images unclean (low SNR).
3. Intrinsic redundancy of a Fourier transform hologram is not sufficient in actual recording, and the reconstructed images are not completely insensitive to dust or scratches (low redundancy and SNR).

Iwamoto proposes using an artificial diffuser which looks like ground glass to control the diffusers optical characteristics. Iwamoto describes a method for generating artificial diffusers characterized by [12:215]:

1. High SNR.
2. High resolution of the reconstructed image.



Figure 18. An F-15 and Tape (above) and its Output (below). The Inversion is Due to Imaging the Original Object onto the CCD Camera.

3. High immunity to dust and scratches.

Iwamoto provides the governing theory on producing an artificial diffuser with optimum spectral distributions. The realized optimum pattern for the diffuser is generated on a computer and plotted. The plot contains an assorted array of small dark spots. This plot is transferred to a phase variation by conventional photographic bleaching process. Iwamoto describes and improved SNR of 8 dB over conventional artificial phase diffusers and a resolution of over 1000 TV lines [12:219].

Diffusers with custom characteristics can be generated and reduced onto glass plates similar to the process for reducing the CT CGH described in Appendix A. The extra step of bleaching the recording would produce the final phase diffuser.

6.3.3 Demonstration of Distortion Invariance To demonstrate the distortion invariant property of the HAM in light of the input shift problem, a template of an F-15 with small tape strip is stored in the memory. The object and it associated output is shown if Figure 18.



Figure 19. An F-15 With Tape Removed (above) and the Associated Output (below). The Inversion is Due to Imaging the Original Object onto the CCD Camera.

The tape is removed and the associated output is shown in Figure 19. The complete stored object is recalled when presented with the distorted, tape removed, input. The graininess of the photographs is due to the slow integration artifact of the CCD camera at low light levels.

6.4 Summary

The major thrust of this thesis is to investigate and characterize the operation of the holographic associative memory and then implement the PSRI variant. The HAM was constructed and one object stored. During the investigation process, a problem with the shift invariance of the input object was found. Minor movements in the input caused the reconstructed reference to vanish. The cause of this problem is a combination of the limiting diameter of the lens and the high diffuse properties of the ground glass. When the input is moved the lens "sees" a new and different object which does not correspond to a stored reference for reconstruction. A larger lens and/or an artificial diffuser with custom optical properties should alleviate this

problem so angle multiplexed holograms can be formed.

The distortion invariant nature of the memory was demonstrated by attaching a strip of tape to the input slide of an F-15 for holographic storage. The tape was removed for reconstruction and both the tape and F-15 were recalled.

VII. Conclusions and Recommendations

7.1 Conclusions

The theory of the PSRI variant holographic associative memory was successfully developed. The $|F(f_{lnr}, f_{\theta})|$ representation of objects were generated by using a coordinate transform computer generated hologram. The behavior of the self-pumped phase conjugate mirror was characterized and the consistent production of relatively high diffraction efficiency phase holograms has been demonstrated.

A holographic associative memory with one stored object was constructed and was operational. A problem with not having a large diameter lens to capture more of the diffuse input or the characteristics of the diffuser itself caused the system to be very sensitive to any movement of the input. The use of fast optics and an artificial phase diffuser with custom characteristics are suggested to alleviate this problem. The distortion invariant characteristic of the memory is demonstrated by storing a template of an F-15 and a strip of tape. The tape is removed, distorting the input, and the original scene is recalled.

Walrond and Childress have demonstrated excellent results correlating in the PSRI feature space with a classical Vander Lugt filter configuration [23]. Scaled and rotated versions of objects produced good autocorrelation peaks with normal oriented objects stored on the hologram. This success gives hope that the PSRI holographic memory would operate properly if the sensitive movement problem were overcome.

7.1.1 Future Applications The holographic associative memory can be used in any application where a conventional Vander Lugt correlator is used with the distinct advantage of allowing access to the input and correlation domains simultaneously.

An object and its $|F(f_{inr}, f_{\theta})|$ representation can be placed side by side on an input template for storage. The $|F(f_{inr}, f_{\theta})|$ space can be used for interrogating the system with both the $|F(f_{inr}, f_{\theta})|$ and the object being recalled for identification. Such a scenario has direct applications to identifying objects from synthetic aperture radar (SAR) imagery.

7.2 Recommendations

For continued research with the PSRI holographic associative memory, the following areas must be further investigated:

1. An investigation of the properties of diffusers must be made and an artificial diffuser constructed as proposed by Iwamoto [12].
2. A large diameter, short focal length lens should be obtained. This will allow more of the diffuse light to be captured in the Fourier transform.
3. When the shift sensitivity is overcome, the multiple stored object memory and the PSRI variant should be fully investigated as outlined in this thesis.
4. Investigate using $LiNbO_3$ as the holographic storage element.

Appendix A. *The Computer Generated Hologram*

A.1 *Introduction*

The $\ln r, \theta$ coordinate transform (CT) is performed by the combination of a computer generated hologram (CGH) and a transform lens. This appendix presents the governing equations for the CT CGH and the methodology for its creation. A detailed discussion of the theory behind the CT CGH is given by Mayo in reference [16]. Much of the following is adapted from this reference [16].

A.2 *Background and Generation*

The CGH is a binary fringe pattern recorded on a high resolution glass plate. The CGH is a simulated recording of a specific wave front with a plane reference or carrier. The CGH will produce many diffracted waves when illuminated, therefore a sufficiently high carrier frequency must be chosen to separate the first diffracted order of the coordinate transform. To avoid this overlap, the following equation must be satisfied for the carrier frequency α :

$$\alpha > \left[\frac{3}{\lambda f_L} \right] \ln \left[\left(\frac{1}{2} x_{max} \right)^2 + \left(\frac{1}{2} y_{max} \right)^2 \right]^{\frac{1}{2}} \quad (33)$$

Where x_{max} and y_{max} are input dimensions, λ is the wavelength, and f_L is the focal length of the lens used.

The CGH used has final dimensions of $x_{max} = y_{max} = 10\text{mm}$, the wavelength is 488.0nm, and the focal length of the lens is 330mm. With these parameters α must be greater than 36.44 lines/mm. An α of 45 lines/mm was used to satisfy the above criteria. The angle θ a plane reference beam would strike the hologram if the CGH were produced optically is 1.26 degrees and is given by the relation:

$$\theta = \arcsin(\alpha\lambda) \quad (34)$$

To create the CT CGH, this carrier must be mixed with the appropriate wavefront whose combined binary fringe pattern is recorded. The transmittance function is the recording of this reference with the following phase function:

$$\phi(x, y) = \left[\frac{2\pi}{\lambda f_L} \right] \left[\ln(x^2 + y^2)^{\frac{1}{2}} - y \arctan(y/x) - x \right] \quad (35)$$

yielding:

$$t(x, y) = 0.5 [1 + \cos(2\pi\alpha x - \phi(x, y))] \quad (36)$$

The transmittance function has maximums where the argument of the cosine satisfies:

$$2\pi\alpha x - \phi(x, y) = 2\pi n_k \quad (37)$$

for integer values of n_k , where each k corresponds to a different fringe.

This equation is used to generate a 128 by 128 array of numbers of the maximums at evenly spaced intervals. The METALIB program on the AFIT/ENP Sun Workstation, is used to draw the contours based on these numbers which results in the CT CGH. A description of the program is given at the end of this appendix. These contours are then printed on the Imagen Laser printer. An example is seen in Figure 20.

A photographic negative of this laser plot was obtained from the Base Photo Lab. The negative was taken to the Cooperative Electronics Materials Process Lab, room 1065 of building 125, to be reduced onto a high resolution glass plate. The Dekacon optical system used for reduction of the CGH is shown in Figure 21.

A 5-inch Wray lens is used in the system to perform a 20x reduction yielding the final CGH dimensions of 10mm by 10mm. Front and rear box settings were 49.97 and 70.05 respectively. The scratched glass plate, scratched surface toward the object screen, is placed in the camera and the CGH was placed onto the object

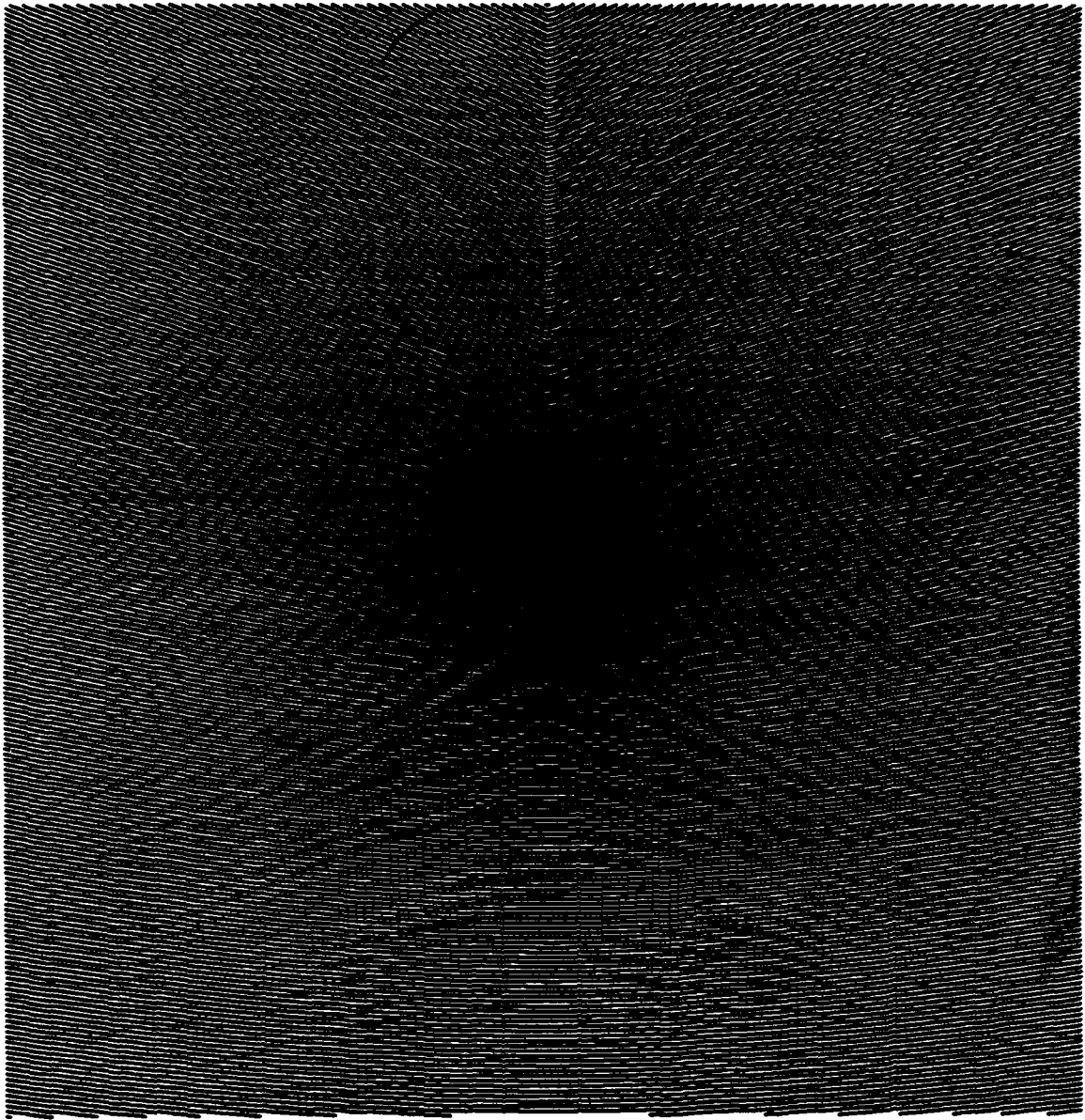


Figure 20. Laser Printer Plot of the CGH.

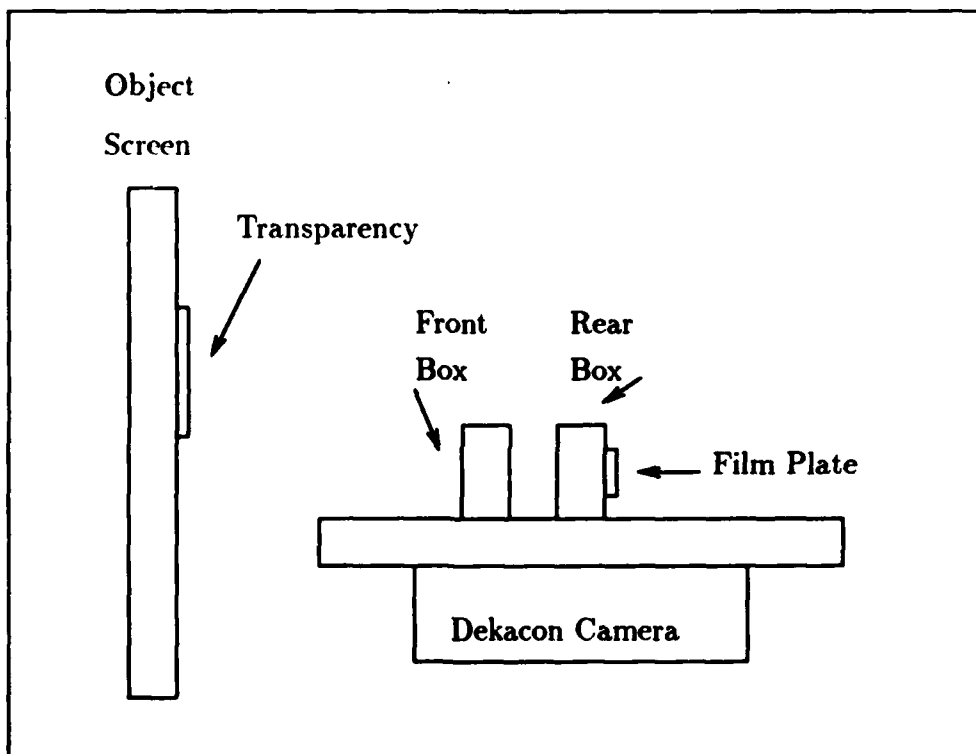


Figure 21. Dekacon Camera System Used to Photoreduce the CGH onto Glass Slides.

screen. When both plate and CGH negative are brought into focus while looking through the aligning microscope, the camera system is properly focused.

With the camera system focused, a 2 x 2 in high resolution glass plate is placed into the camera with the emulsion side toward the object screen. The shutter is removed from the plate holder and the plate is exposed for 4 minutes. This differed from Mayo's reported 40-60 second exposure times. After exposure, the plates are then brought to the darkroom for development. The plate is placed in the developer for 5 minutes, with the solution vibrator on. The plate is then placed in the stop bath for 20 seconds, fixer for 1 minute and a final rinse in deionized water for 30 seconds. After the rinse, the plate was dried with a jet of air. These exposure and development times may vary depending on the age of the developer. The final CGH had distinct clear and opaque lines when viewed under a microscope.

A.3 The computer program

The generation of the CT CGH was done by using a Fortran program to produce the 128 by 128 array of numbers corresponding to the fringe maxima. The contours defined by these values were drawn by the RCONTR program of MET-ALIB. The program used to plot the CT CGH is shown below.

```
C
C ***** LN R.THETA INTERFEROGRAM *****
C
      real    SURFAC(128,128), X, Y, ALPHA, LAMDA, FOCAL, TEMP, PI,
      + INCX, INCY, CONTV(2), KS, Xcoord(128), Ycoord(128)
integer ICTRS
C
ICTRS = 0
KS = -400.0 'not needed--returns number of lines plotted
```

```
CONTV(1) = -350.0 'set to minimum value in array
          CONTV(2)      = .6      'delta value
```

```
C
```

```
X = -2.51 'minimum dimension of CGH
Y = -2.51 'minimum dimension of CGH
ALPHA = 45.0 'Angle of plane reference
FOCAL = 330 'focal length of associated lens
LAMDA = 0.0004880 'wavelength
INCX = 5.0 / 128.0 'step increment of x
INCY = 5.0 / 128.0 'step increment of y
PI = 3.1415926
```

```
C
```

```
do 10 j = 1, 128, 1 'this loop generates data
  do 20 i = 1, 128, 1
    if ( (X.lt.0) .and. (Y.gt.0) ) then
      TEMP = X*0.5*log(X*X+Y*Y)-Y*(PI+atan(Y/X))-X
    else if ( (X.lt.0) .and. (Y.lt.0) ) then
      TEMP = X*0.5*log(X*X+Y*Y)+Y*(PI-atan(Y/X))-X
    else
      TEMP = X*0.5*log(X*X+Y*Y)-Y*atan(Y/X)-X
    end if
    SURFAC(i,j) = ALPHA*X - (1/(LAMDA*FOCAL))*TEMP
    Xcoord(i) = X
    X = X + INCX
  20 continue
  Ycoord(j) = Y
  X = -2.51
  Y = Y + INCY
```

```

10 continue
C
C **** METALIB Subroutines *** (described in manual)
C
call setplot( "lnplot128", 7, 0, .false.)
C
call mapxy( -2.51, 2.49, -2.51, 2.49, 0.0, 0.7, 0.0, 0.9, 0, 1 )
C
      call rcontr( ICTRS, CONTV, KS, SURFAC, 128, Xcoord, 1, 128, 1,
+      Ycoord, 1, 128, 1, .false. )
C
call endplot
C
      end

```

The function of the METALIB subroutines SETPLOT, MAPXY and END-PLOT are explicitly explained in the METALIB manual. In the RCONTR subroutine, the role of ICTRS, CONTV(1), CONTV(2), and KS can be confusing. With $ICTRS = 0$ all contours of the form $CONTV(1) + m * CONTV(2)$, m determined by METALIB, are drawn. METALIB assumes $CONTV(1)$ contains a starting value and $CONTV(2)$ a delta value. It is computationally economical to set $CONTV(1) = \min SURFAC(X,Y)$, however it may be set to any value below $\min SURFAC(X,Y)$ but not above. $CONTV(2)$ controls the density of the plot. METALIB increments on $CONTV(2)$ to draw contours by interpolating between values given in $SURFAC(X,Y)$. $CONTV(2)$ must be adjusted to fit the specific conditions of wavelength, alpha, focal length, and plot dimensions. $CONTV(2) = .6$ gave the best results for the parameters used.

Appendix B. *Samples of the PSRI Feature Space*

B.1 Introduction

This appendix shows the results of the generation of the PSRI feature space discussed in Chapter 3. Each photograph depicts the original object, its Fourier transform, and the $|F(f_{inr}, f_{\theta})|$ representation.

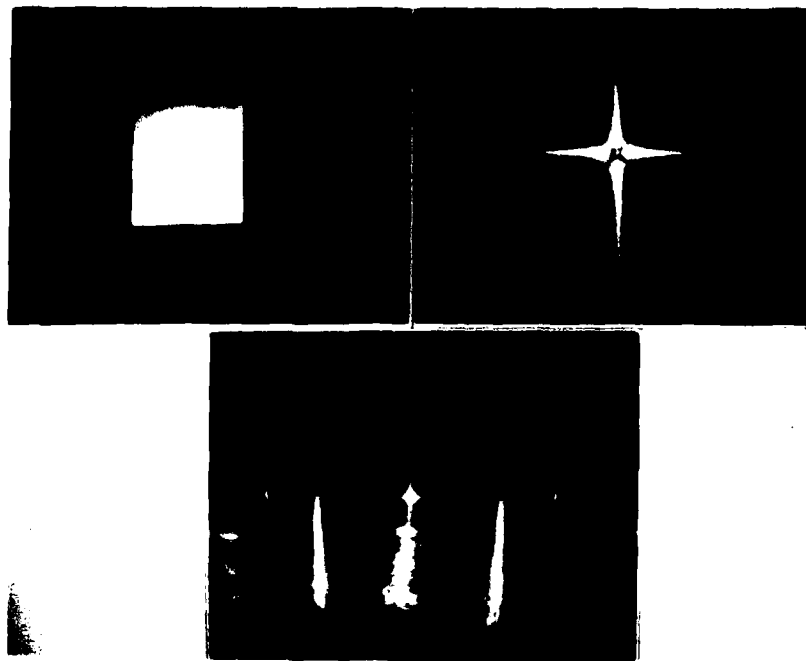


Figure 22. The Large Square.

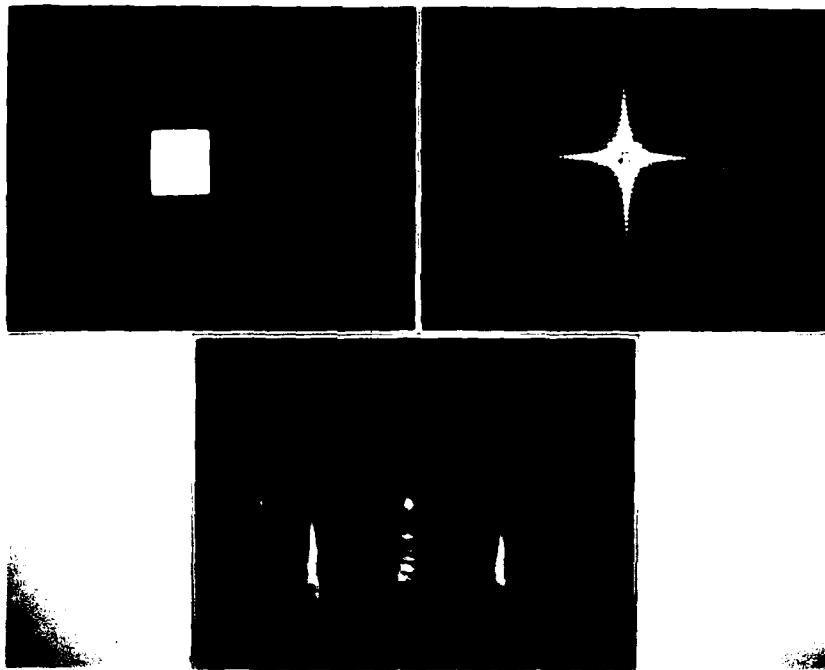


Figure 23. The Small Square.

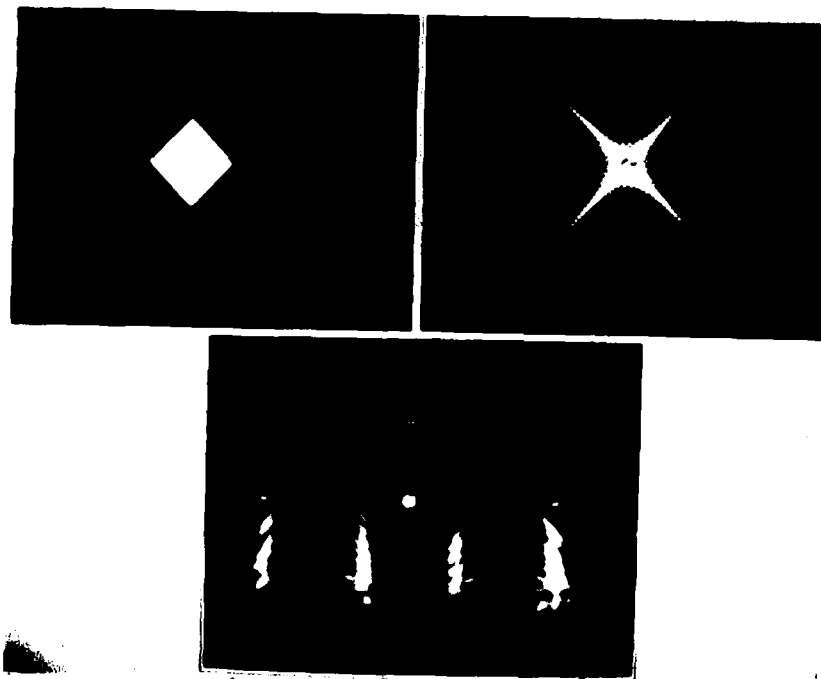


Figure 24. The Small Square Rotated 45 Degrees.

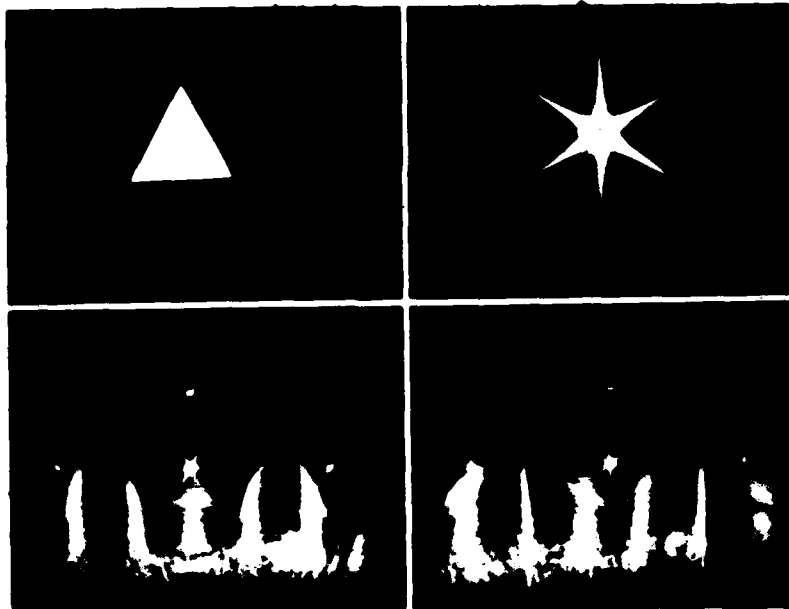


Figure 25. The Triangle Normal and Rotated 30 Degrees.

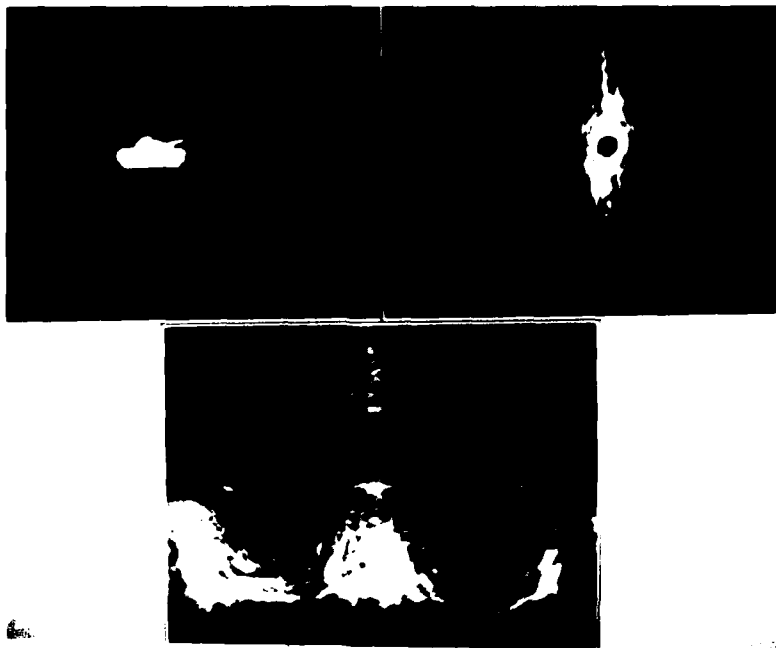


Figure 26. The Small Tank.

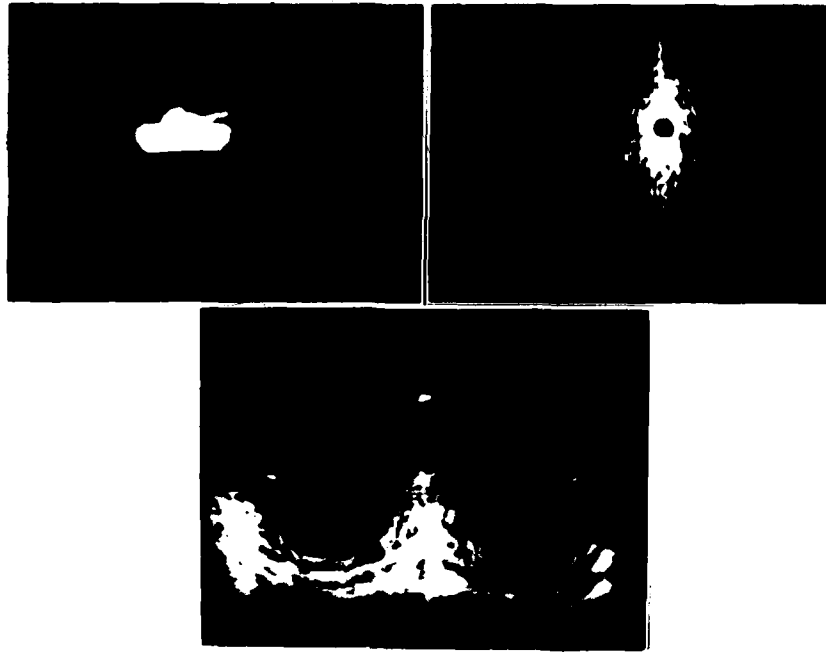


Figure 27. The Large Tank.

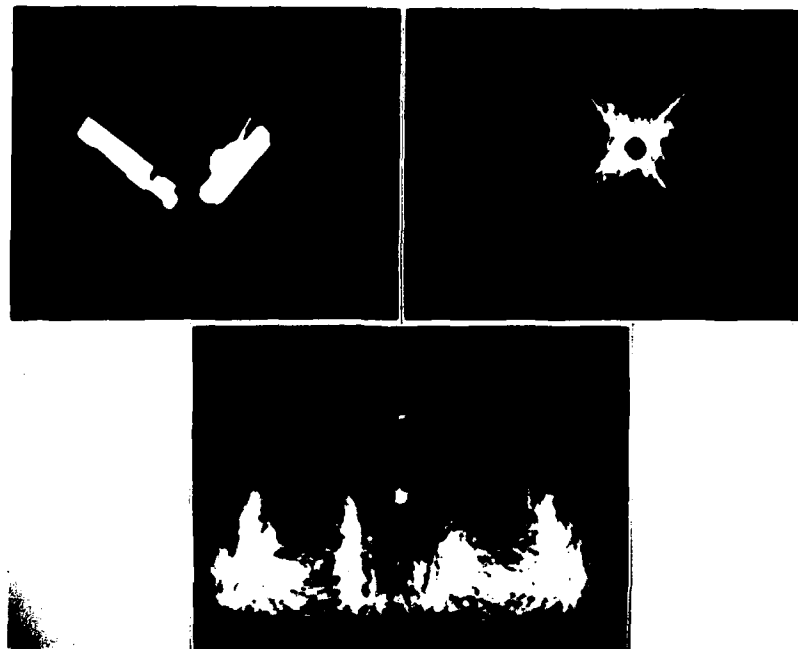


Figure 28. The Truck and Tank at 90 Degrees.

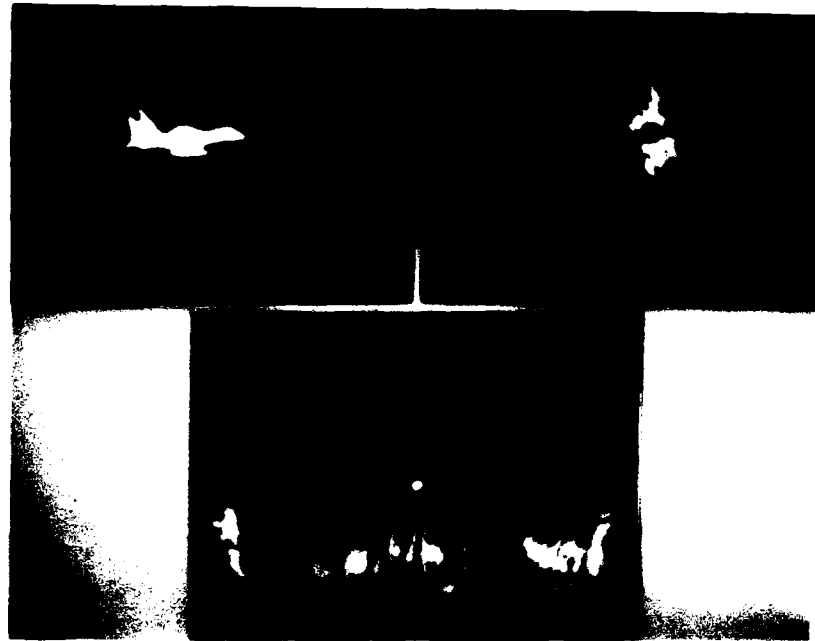


Figure 29. The Small F-15.

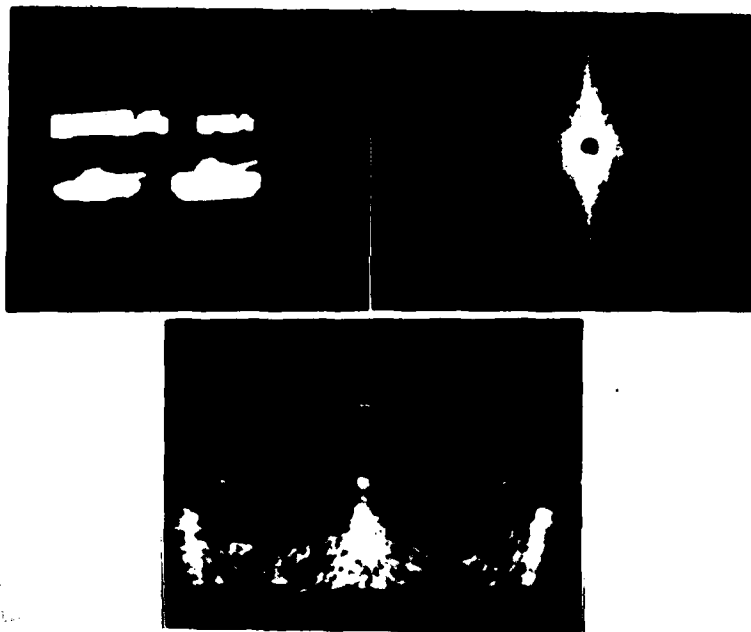


Figure 30. Two Trucks and Two Tanks.

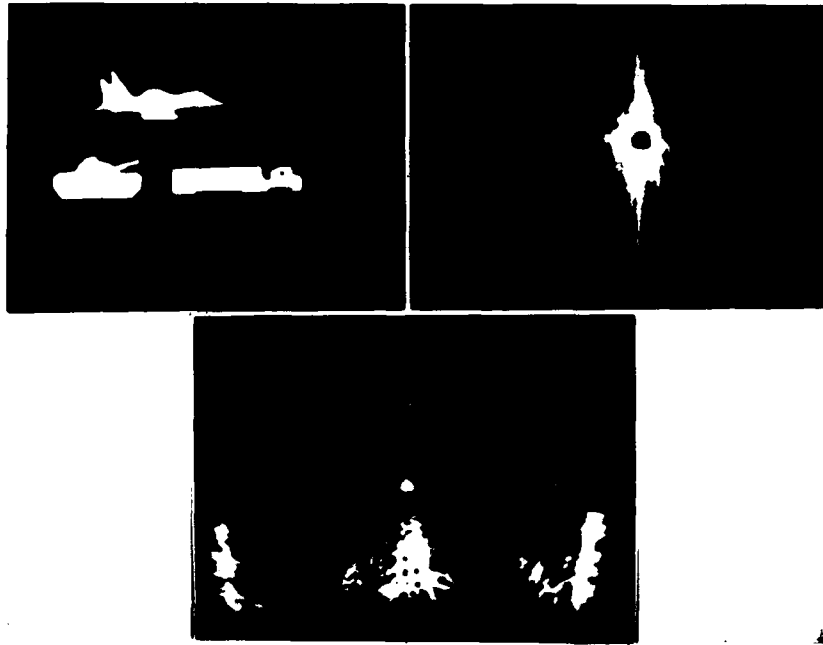


Figure 31. Truck, Tank, and F-15.

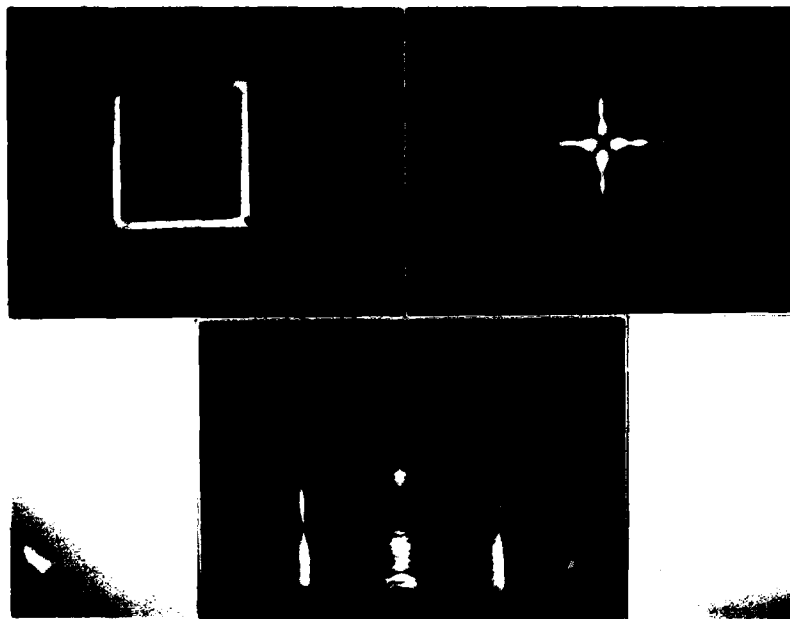


Figure 32. The Large Edged Square.

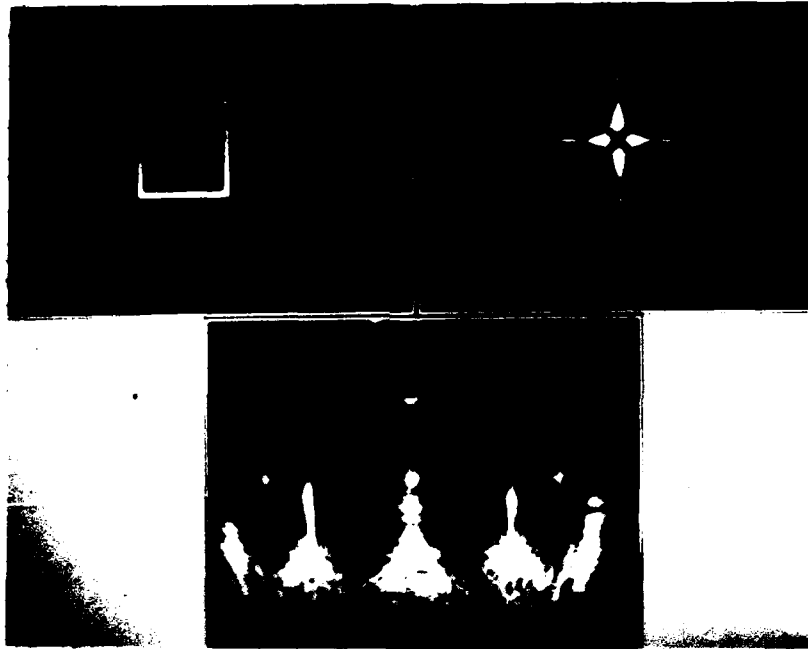


Figure 33. The Small Edged Square.

Bibliography

1. Anderson, D. Z. "Coherent Optical Eigenstate Memory," *Optics Letters*, 11: 45 (1986)
2. Casasent, David and Demetri Psaltis. "Position, Rotation, and Scale Invariant Optical Correlation," *Applied Optics*, 7: 1795-1799 (July 1976).
3. Collier, Robert J. et al. *Optical Holography*. New York: Academic Press, 1971.
4. Collier, Robert J. and K. S. Pennington. "Ghost Imaging by Holographic Forms in the Near Field," *Applied Physics Letters*, 8: 44 (1986).
5. Cronin-Golomb, Mark et al. "Passive (self-pumped) Phase Conjugate Mirror: Theoretical and Experimental Investigation," *Applied Physics Letters*, 41: 689-691 (October 1982).
6. Cronin-Golomb, Mark and Amnon Yariv. "Phase Conjugate Mirrors as Thresholding Elements for Optical Associative Memories," *SPIE-International Optical Computing Conference*, 700: 301-303 (1986).
7. Dunning, G., Electrical Engineer. Telephone Interview. Hughes Research Corporation, Malibu, CA, 10 October 1988.
8. Dunning, G. et al. "All-optical Associative Memory with Shift Invariance and Multiple-image Recall," *Optics Letters*, 12: 346-348 (May 1987).
9. Feinberg, Jack. "Self-pumped Continuous-wave Phase Conjugation using Internal Reflection," *Optics Letters*, 7: 486-488 (October 1982).
10. Fischer, Baruch. et al. "Amplified Reflection, Transmission and Self-Oscillation in Real-Time Holography," *Optics Letters*, 6: 519-521 (November 1981).
11. Hariharan, P. and C. M. Chidley. "Photographic Phase Holograms: Spatial Frequency Effects with Conventional and Reversal Bleaches," *Applied Optics*, 27: 3065-3067 (August 1988).
12. Iwamoto, Akito. "Artificial Diffuser of Fourier Transform Hologram Recording," *Applied Optics*, 19: 215-221 (January 1980).
13. Kwong, Sze-Keung and Amnon Yariv. "Bistable Oscillations with a Self-Pumped Phase-conjugate Mirror." *Optics Letters*, 11: 378-379 (June 1986).
14. MacDonald, Kenneth R. and Jack Feinberg. "Theory of Self-pumped Phase Conjugator with Two Coupled Interaction Regions," *Journal of the Optical Society of America*, 73: 548-553 (May 1983).
15. Marom, E. and J. W. Goodman. "Ghost Image Interferometry," *Applied Optics*, 17: 45 (1978)
16. Mayo, 2Lt Michael W. *Computer Generated Hologram and Magneto-Optic Spatial Light Modulator for Optical Pattern Recognition*. MS Thesis,

AFIT/GEO/ENG/87D-1. School of Engineering, Air Force Institute of Technology (AU), Wright-Patterson AFB, OH, December 1987. (DTIC number not available at this time).

17. Nakayama, Yoshikazu and Makoto Kato. "Linear Recording of Fourier Transform Holograms Using a Pseudorandom Diffuser," *Applied Optics*, 21: 1410-1418 (April 1982).
18. Owechko, Y. et al. "Holographic Associative Memory with Nonlinearities in the Correlation Domain," *Applied Optics*, 26: 1900-1910 (May 1987). Feedback Using Phase Conjugate Mirrors," *Optics Letters*, 11: 118-120 (February 1986).
19. Smout, A.M.C. and R. W. Eason. "Regular Oscillations and Self-pulsating in Self-pumped $BaTiO_3$," *Optics Communications*, 59: 77-82 (August 1986).
20. Soffer, B.H. et al. "Associative Holographic Memory with Feedback Using Phase Conjugate Mirrors," *Optics Letters*, 11: 118-120 (February 1986).
21. Soffer, B.H. et al. "Holographic Associative Memory Employing Phase Conjugation," *SPIE-International Society of Optical Engineering*, 684: 2-6 (July 1986).
22. White, H. J. et al. "Digital and Analogue Holographic Associative Memories," *Optics Letters*, 11: 30-37 (January 1988).
23. Walrond, Capt Thomas and Capt Timothy Childress. *Position, Scale, and Rotation Invariant Optical Pattern Recognition For Target Extraction and Identification*. MS Thesis, AFIT/GE/ENG/88D-4. School of Engineering, Air Force Institute of Technology (AU), Wright-Patterson AFB, OH, December 1988.
24. Wilson, Capt Jeffery A. *Optical Information Processing in a Confocal Fabry-Perot Resonator*. MS Thesis, AFIT/GEO/ENG/88D-5. School of Engineering, Air Force Institute of Technology (AU), Wright-Patterson AFB, OH, December 1988.
25. Yariv, Amnon and S. K. Kwong. "Associative Memories Based on Message Bearing Optical Modes in Phase Conjugate Resonators," *Optics Letters*, 11: 186 (1986).

Vita

Kenneth H. Fielding [REDACTED]

He graduated from Jacksonville High School in Jacksonville, Arkansas in 1979. He attended the University of Central Arkansas in Conway, Arkansas where he earned a Bachelor of Science degree in Physics in May 1983. He immediately entered the USAF Officer Training School and was commissioned a Second Lieutenant in August 1983. Lt Fielding's first assignment was to attend the University of New Mexico, in Albuquerque, New Mexico for the Air Force Institute of Technology, Undergraduate Engineering Conversion Program earning a Bachelor of Science in Electrical Engineering. He graduated with Distinction in May 1985. Lt Fielding was assigned to the Tactical Air Warfare Center (TAC) at Eglin AFB, Florida where he served as an Electronic Warfare Engineer. In May 1987, he entered the Electro-Optics Masters Program in the School of Engineering, Air Force Institute of Technology.

[REDACTED]

UNCLASSIFIED

SECURITY CLASSIFICATION OF THIS PAGE

REPORT DOCUMENTATION PAGE

Form Approved
OMB No. 0704-0188

1a. REPORT SECURITY CLASSIFICATION UNCLASSIFIED		1b. RESTRICTIVE MARKINGS	
2a. SECURITY CLASSIFICATION AUTHORITY		3. DISTRIBUTION/AVAILABILITY OF REPORT Approved for public release; distribution unlimited	
2b. DECLASSIFICATION/DOWNGRADING SCHEDULE		4. PERFORMING ORGANIZATION REPORT NUMBER(S) AFIT/GEO/ENG/88D-2	
5. MONITORING ORGANIZATION REPORT NUMBER(S)		6a. NAME OF PERFORMING ORGANIZATION School of Engineering	
6b. OFFICE SYMBOL (If applicable) AFIT/ENA		7a. NAME OF MONITORING ORGANIZATION	
6c. ADDRESS (City, State, and ZIP Code) Air Force Institute of Technology Wright-Patterson AFB, OH 45433		7b. ADDRESS (City, State, and ZIP Code)	
8a. NAME OF FUNDING/SPONSORING ORGANIZATION Rome Air Development Center		8b. OFFICE SYMBOL (If applicable) RADC/COTC	
9. PROCUREMENT INSTRUMENT IDENTIFICATION NUMBER		10. SOURCE OF FUNDING NUMBERS	
8c. ADDRESS (City, State, and ZIP Code) Rome Air Development Center Griffiss AFB, NY 13411		PROGRAM ELEMENT NO.	PROJECT NO.
		TASK NO.	WORK UNIT ACCESSION NO.
11. TITLE (Include Security Classification) A Position, Scale, and Rotation Invariant Holographic Associative Memory UNCLASSIFIED			
12. PERSONAL AUTHOR(S) Fielding, Kenneth Henry, Capt, USAF			
13a. TYPE OF REPORT MS Thesis	13b. TIME COVERED FROM _____ TO _____	14. DATE OF REPORT (Year, Month, Day) 1988 December	15. PAGE COUNT 76
16. SUPPLEMENTARY NOTATION			
17. COSATI CODES		18. SUBJECT TERMS (Continue on reverse if necessary and identify by block number)	
FIELD	GROUP	SUB-GROUP	
17	05	Optical storage; holography; associative memory	
19. ABSTRACT (Continue on reverse if necessary and identify by block number) Thesis Chairman: Steven K. Rogers, Capt, USAF Associate Professor of Electrical and Computer Engineering This thesis investigates an all-optical position, scale, and rotation invariant (PSRI) holographic associative memory employing phase conjugation. The PSRI feature space is the in-polar representation of the magnitude of the Fourier transform of the objects. This representation is generated using a coordinate transform computer generated hologram. Diffuse Fourier transform holograms of the PSRI feature space and the use of angularly multiplexed references allow access to the correlation domain where the nonlinear properties of the phase conjugate mirror (PCM), self-pumped barium titanate, reduces cross-correlation noise and provides object discrimination. The self-pumped PCM is characterized and a procedure for the consistent production of high diffraction efficiency holograms is developed. The holographic associative memory is constructed and its operational parameters are defined.			
20. DISTRIBUTION/AVAILABILITY OF ABSTRACT <input type="checkbox"/> UNCLASSIFIED/UNLIMITED <input checked="" type="checkbox"/> SAME AS RPT <input type="checkbox"/> DTIC USERS		21. ABSTRACT SECURITY CLASSIFICATION UNCLASSIFIED	
22a. NAME OF RESPONSIBLE INDIVIDUAL Capt Steven K. Rogers		22b. TELEPHONE (Include Area Code) 513-255-6027	22c. OFFICE SYMBOL AFIT/ENG

DD Form 1473, JUN 86

Previous editions are obsolete.

SECURITY CLASSIFICATION OF THIS PAGE

UNCLASSIFIED